공학석사 학위논문

고연소도 피복관 연성평가방법론에 대한 실험적 탐구 및 연성 기반과 파단 기반 안전기준의 비교 분석

Experimental investigation of ductility assessment methods for high burnup fuel cladding and comparative analysis of ductility-based and fracture-based safety criteria

2022년 8월

서울대학교 대학원

에너지시스템공학부 원자핵공학전공

금 경 환

고연소도 피복관 연성평가방법론에 대한 실험적 탐구 및 연성 기반과 파단 기반 안전기준의 비교 분석

Experimental investigation of ductility assessment methods for high burnup fuel cladding and comparative analysis of ductility-based and fracture-based safety criteria

지도교수 이 유 호

이 논문을 공학석사 학위논문으로 제출함

2022년 8월

서울대학교 대학원

에너지시스템공학부 원자핵공학전공

금 경 환

금경환의 공학석사 학위논문을 인준함

2022년 8월

위 원 장 조 형 규 (인)

부위원장 박 현 선 (인)

위 원 이 유 호 (인)

Abstract

Experimental investigation of ductility assessment methods for high burnup fuel cladding and comparative analysis of ductility-based and fracture-based safety criteria

Kyunghwan Keum

School of Energy Systems Engineering

The Graduate School

Seoul National University

Technical basis of establishment on acceptance criteria for emergency core cooling systems(ECCS) on high-burnup cladding is systemically studied.

Two main experiments, thermal shock fracture and post-quench ductility based experiments were compared to explain discrepancy between each ECR limits of high burnup claddings. Using MARS, GIFT code, cladding temperature, stress, amount of precipitated Hydrogen during LOCA transient were calculated. During LOCA, at the timing of reflood quenching, cladding stress reaches highest point at ~ 200℃. At that critical moment, precipitated amount of Hydrogen is remained at low level due to its precipitation kinetics. In post-quench ductility experiment, ring compression test(RCT) is done at 135℃, with all the hydrogen is in precipitated state. This difference in temperature and precipitated amount of hydrogen resulted in difference of ECR limit.

Detailed conditions in post-quench ductility experiments were investigated. Cooling rate before quench and quench temperature, cooling water temperature, RCT crosshead speed, RCT temperature, specimen length was systemically studied.

Slow cooling rate before quench resulted in partitioning of alloying elements and longer hydride formation, which increased cladding ductility. Cooling rate during quench, controlled by subcooling of quenching water, showed limited effect on residual ductility of the cladding, while thermal shock has been strengthen by fast cooling rate with -75℃ subcooled water. Crosshead speed of 2mm/min was shown to be enough slow speed which cladding ductility is not affected by slowing down or speeding up the RCT speed. Increased RCT temperature apparently increased cladding ductility. specimen length 8mm was suggested to limit the length effect on residual ductility.

Embrittlement limit of HANA and ZIRLO cladding was derived. They showed slightly lower ECR limit in 50~250wppm cladding compared to U.S.NRC draft rule, while 400wppm~650wppm cladding showed similar results with draft rule. RCT temperature shift was suggested to fill the gap between draft rule and SNU limit. RCT temperature of 185℃ was anticipated to fill the gap between two limit.

With the conclusions of this study, current regulatory experimental protocols assessing leftover ductility of cladding after LOCA was revisited. Regulatory authorities should have lenient perspective on experimental conditions and methods, to make realistic regulatory criteria for emergency core cooling system.

Keyword : High-burnup
Loss of Coolant Accident
Hydride
ECCS criteria
Ductility
Thermal shock fracture

Student Number : 2020-23056

Table of Contents

Abstract 3

Chapter 1. Introduction 11

1.1. Cladding behavior during LOCA transient 12
1.2. ECCS criteria for high-burnup cladding 17
1.3. Thesis objectives and organizations 19

Chapter 2. Comparison between Thermal Shock Fracture and Post-LOCA Ductility Based ECCS Criteria 20

2.1. Technical base for Thermal shock fracture based and post-LOCA ductility based ECCS criteria 21
2.2. Method 26
2.3. Results and discussions 28
2.4. Conclusion 30

Chapter 3. Analyzing protocols of LOCA post-quench ductility experiments. 31

3.1. Experimental procedures for post-quench ductility based criteria 32
3.2. Cooling rate and quenching temperature 37
3.3. Quenching water temperature effect 49
3.4. Ring Compression Test strain rate 62
3.5. Ring Compression Test temperature 65
3.6. Specimen length 67
3.7. Conclusion 69

Chapter 4. Embrittlement limit of pre-hydrided ZIRLO and HANA claddings. 71

4.1. Deriving embrittlement limit of pre-hydrided ZIRLO and HANA claddings. 72
4.2. RCT in different temperature 77
4.3. Conclusion 80

Chapter 5. Summary of Conclusions 81

5.1. Summary of conclusions 82

List of Figures

Figure 1-1. Fuel cladding temperature history during LOCA 13

Figure 1-2. Schematic diagram of fuel cladding after high temperature oxidation 14

Figure 1-3. Zr-O phase diagram..... 14

Figure 1-4. Embrittlement limit for high-burnup cladding(USNRC) 18

Figure 2-1. Hobson's RCT facility 22

Figure 2-2. Embrittlement limit derived from Hobson's experiment. 22

Figure 2-3. Uetsuka's LOCA facility and fracture shape after integral testing..... 23

Figure 2-4. Temperature history and load curve in Uetsuka's experiment 24

Figure 2-5. Ductility limit for thermal shock fracture based experiment. (a) unrestrained condition, (b) fully restrained condition 24

Figure 2-6. Ductilit and thermal shock fracture based criteria for high-burnup claddings..... 25

Figure 2-7. Schematic for Code-integrated LOCA analysis 26

Figure 2-8. Stress convergence results for each direction 27

Figure 2-9. LBLOCA analysis of UCN 3&4. (a) Axial location 1.17m, (b) axial location 2.99m 28

Figure 2-10. JAEA and U.S. NRC LOCA experiment analysis 30

Figure 3-1. Experimental protocol suggested in U.S.NRC regulatory guide.....32

Figure 3-2. Two different methods to analyze RCT results and derive ECR limit.....34

Figure 3-3. (a) Hydrogen charging apparatus, (b) hydride morphology of ZIRLO cladding captured with optical microscopy.....35

Figure 3-4. Schemetic of LOCA apparatus 36

Figure 3-5. Four different tested cooling modes and corresponding temperature history 39

Figure 3-6. Demonstration for Hydrogen content measurement 40

Figure 3-7. 4 Load-Displacement curve of Different temperature history 41

Figure 3-8. EBSD analysis results (Inverse Pole Figure(IPF), grain size distribution) for four different cooling conditions.....
44

Figure 3-9. Pole figure of (a) as-received ZIRLO specimen, (b) after 1200°C, 60s oxidation. 45

Figure 3-10. Hydride morphology for four different cooling conditions. 46

Figure 3-11. . (a) Phase analysis and kikuchi pattern analysis for (b) γ-hydride and (c) δ-hydride 47

Figure 3-12. Temperature history during LBLOCA. 48

Figure 3-13. Microstructure change with cooling rate 48

Figure 3-14. Optical microscopy of hydride distribution..... 52

Figure 3-15. EDS Oxygen distribution of ~17% ECR at 1204°C.. 52

Figure 3-16. Phase layer thickness of specimens oxidized to 17% ECR at 1204°C 53

Figure 3-17. veraged oxygen content of each phase layer of specimens oxidized to 17% ECR at 1204°C..... 54

Figure 3-18. Metallographic Analysis of post-LOCA Zircaloy-4 specimens..... 55

Figure 3-19. Boiling modes of Zircaloy-4 quenched into (a) 100oC water (saturated) (b) 25 oC water. 57

Figure 3-20. Vicker's hardness measurements of each phase layer.... 58

Figure 3-21. Load-displacement curves of Ring Compression Test results. 58

Figure 3-22. DIC results of von-Mises Strain for as-received Zircaloy-4 specimens (~17% ECR at 1204°C) undergoing RCT at 135°C 60

Figure 3-23. Measured Ring Compression Test parameters with various strain rate 63

Figure 3-24. RCT results for different temperatures. 66

Figure 4-1. Derived ductile ECR limit from RCT offset strain results of (a) SNU, (b) CEA 74

Figure 4-2. Ductile limit derived from pre-hydrided ZIRLO, HANA cladding 75

Figure 4-3. 150℃, 170℃, 190℃ temperature RCT results for (a) 100wppm, (b) 200wppm, (c) 250wppm, (d) 300wppm 78

Figure 4-4. Deriving ductile temperature limit for cladding at ductile-brittle boundary 78

Figure 4-5. Comparing SNU-ECR limit with RCT results of different temperatures. 79

List of Tables

Table 1-1. Acceptance Criteria for Emergency Core Cooling System (10 CFR 50.46 from U.S. NRC) 12

Table 1-2. Exepriment protocols for establishing ECCS criteria 16

Table 3-1. Composition of ZIRLO cladding 37

Table 3-2. High temperature oxidation and RCT results for different cooling rate using pre-hydrided(PH) 159.8±23.1wppm and as-received(AR) ZIRLO specimen. 42

Table 3-3. Summary of RCT results 59

Table 3-4. Suggested LOCA experiment and RCT protocols in this study 70

Table 4-1. Ductile test results of different Hydrogen content and different ECR. Each line indicates the average of three 8mm specimens. 72

Table 4-2. Comparison between different experiment facilities, ANL/CEA/SNU 76

Table 4-3. Ductile test results of different Hydrogen content with embrittlement limit ECR. Each line indicates the average of three 8mm specimens. 77

Chapter 1. Introduction

1.1. Cladding behavior during LOCA transient

Nuclear fuel cladding in light water reactor plays a role as a primary barrier for nuclear safety, by preventing the leak of uranium fuel and fission products. Not only for the normal operation state, should fuel cladding maintain its integrity during accident situations.

Acceptance criteria for emergency core cooling system (ECCS) are very important regulatory requirements in designing nuclear reactors. Acceptance criteria, which can be replaced by the word of 'performance criteria' for ECCS, are evaluated by the ability to prevent the loss of coolant accident (LOCA) from accident to progress into severe accident. As a requirement, maintaining of the integrity of a fuel cladding during LOCA is required, as shown in table 1.

Table 1-1. Acceptance Criteria for Emergency Core Cooling System (10 CFR 50.46 from U.S. NRC)

Lists	Accetpance Criteria	Purpose
Peak Cladding Temperature(PCT)	**Under 2200°F(1204°C)**	Prevent breakaway oxidation
Equivalent Cladding Reacted(ECR)	**Under ECR 17%**	Maintaining cladding integrity
Hydrogen Generation	0.01 times the total hypothetical amount	Prevent hydrogen explosion
Coolable Geometry	Core remains amenable to cooling	Maintainng Core Coolability
Long-Term Cooling	Core temperature maintained at acceptably low value	

Except for the hydrogen generation which can be addressed by limiting the oxidation of the cladding, cladding integrity can be impaired by two modes; ductile and brittle modes. The ductile impairment is accompanied by partial blockage of the fuel assembly channels due to ballooning and burst. This mode is addressed by 'Coolable geometry' and 'Long-term cooling'. It is noteworthy that no quantitative limits are associated with the above criteria. In general, the ductile mode impairment is known to be not significant; experiments demonstrated that a 90% blockage still maintains an acceptable level of coolability, and maximum attainable flow blockage ratio is

found to ~71%. Yet, questions remain on the coolability of blocked bundles with fragmented pellets relocated in ballooned region, and recently there has been increasing interest in investigating it.

Brittle mode has traditionally been the primary regulatory basis for regulation. Limits for peak cladding temperature (PCT) 1204℃ and equivalent cladding reacted (ECR) 17% are aimed to protect cladding ductility during LOCA.

In LOCA situation, cladding experience temperature transient shown in figure 1.1. When Zircaloy cladding is exposed to high temperature steam, it Zr reacts with water molecules and cladding is oxidized, as shown in (1).

$$\mathrm{Zr} + 2H_2O = ZrO_2 + 2H_2 \quad \ldots (1)$$

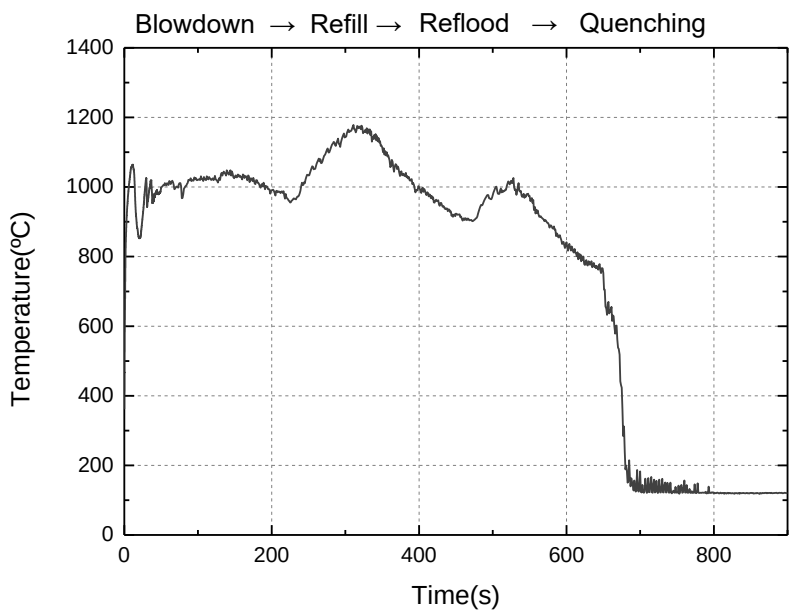

Figure 1-1. Fuel cladding temperature history during LOCA

Cladding has an oxide layer, and an α layer with a certain oxygen concentration, and β layer with the lowest oxygen concentration formed from the part that contacts with the vapor during oxidation. β layer exhibits β phase at a high temperature, but

changes to an α phase when the temperature changes to a low temperature, so it is called the Prior-β layer. A schematic diagram of three phases and oxygen content in the oxidized cladding tube are presented in fig. 1.3.

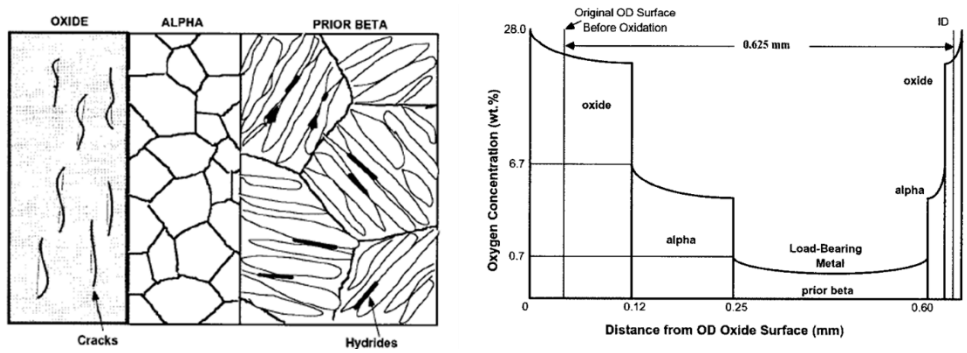

Figure 1-2. Schematic diagram of fuel cladding after high temperature oxidation

Thickness of each phase is decided by oxygen content and temperature. At the same temperature, β phase is dominant if oxygen content gets increase, and α phase is dominant with increase of oxygen content. Phase diagram of Zr-O is shown in figure 1-3.

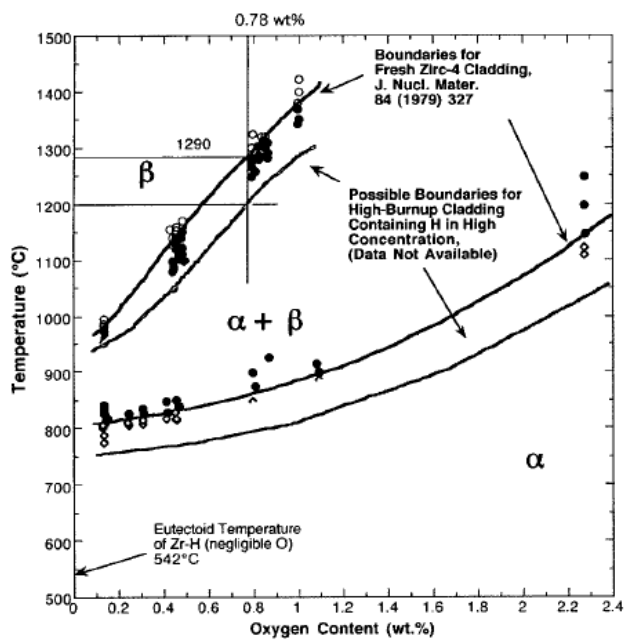

Figure 1-3. Zr-O phase diagram

Hobson has conducted high temperature oxidation and ring compression test using Zircaloy cladding. Results were used in 1973 rule-making hearing to decide peak cladding temperature and oxidation level of the cladding. Thickness of prior-β phase was used to decide ECCS criteria, since prior-β carries most of cladding ductility.

The experiment was conducted on the assumption that the Zirconium cladding tube, whose temperature rose due to decay heat in the event of a LOCA, and additionally heated due to oxidation heat from a oxidation reaction of cladding with steam. Hobson oxidized the cladding tube at a high temperature at a constant temperature, and then quenched the cladding tube heated to high temperature in water which is a surrogate for reflood situation.

These experimental methods and procedures were standardized and presented in the current U.S. NRC Regulatory Guide. In table 1-2, several key factors of regulatory guide is presented. Experimental protocols during LOCA experiment and RCT both has an important meaning in deciding ECCS criteria, and more details for those meanings will be addressed in chapter 3 in this thesis.

Table 1-2. Exepriment protocols for establishing ECCS criteria

LOCA experiment protocols		
	Value	**Physical validity**
Cladding type	Any Zircaloy cladding	Any composition of zircaloy showed similar ductility after oxidation
Specimen length	25mm	To get uniform temperature in same specimen
Heating/cooling rate	Over 20℃/s / over 2℃/s	To simulate LOCA situation
Quenching temperature	1200℃ or 800℃	To simulate reflood situation during LOCA
Quenching water	Not presented	Needs to be revised
Steam flow rate	0.8 mg/cm^2/s ~ 30mg/cm^2/s	Oxidation behavior remains same in this range
Ring compression test protocols		
Stiffness comparison	Measeured stiffness K_m< Theoretical stiffness K_c	To test if the calibration of RCT facility is appropriately done
Strain rate	0.0083 mm/s ~ 0.033mm/s	Stiffness and strength increases with strain rate
RCT temperature	135℃	Temperature after the termination of LOCA
Fracture decision	30% load decrease	Load decrease of 30% represent overall fracture of the cladding
Ductility assessment	1% permanent strain or offset strain ≥ 1.41+0.1082 CP-ECR	Permanent strain 1% indicates sufficient ductility of the specimen
Specimen length	7-10mm	Needs to be revised

JAEA has done different experiment, which uses long length cladding specimen to test integral integrity of the cladding. The top and bottom of the cladding is restrained, to see the thermal shock fracture of the cladding during quench. Despite the difference of test method, they got similar results with Hobson's experiment, and established same LOCA ECCS criteria.

1.2. ECCS criteria for high-burnup cladding

High-burnup cladding has some deteriorated aspects compared to fresh cladding. During operation of the light water reactors, cladding reacts with coolant, and fuel release the radiation. Cladding continuously accumulates oxide layer and hydrogen, and radiation damage. Oxide layer acts as decreased cladding thickness, which means that ductile layer thickness has been decreased by the oxidation. Absorbed hydrogen increases cladding embrittlement, by forming hydrides. This hydrides act as a pre-existing crack. Radiation damage forms various defects to the cladding. Fortunately, in LOCA transient formed defect from radiation is recovered, by high temperature annealing effect. So the main issue for high-burnup cladding in LOCA situation is the pre-existing oxide layer and hydrogen content in the cladding.

Due to the various high-burnup effects on the cladding, several issues have been brought up. The purpose was to quantify the high burnup effects, and respond to the problems. U.S. NRC has done LOCA simulating experiments using high-burnup, and pre-hydrided cladding which is the surrogate for high-burnup cladding. In high-burnup cladding, LOCA ECCS criteria were changed, due to the hydrogen embrittlement effect on the cladding (fig. 1-4).

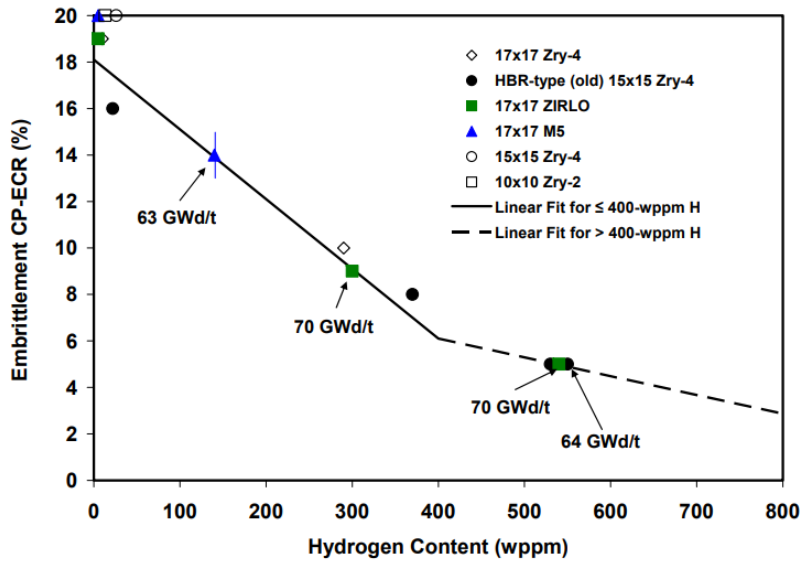

Figure 1-4. Embrittlement limit for high-burnup cladding(USNRC)

In thermal shock fracture experiment (JAEA), high-burnup cladding had little effect on cladding integrity. Same ECR limit was derived for high-burnup cladding and as-received cladding, in this experiment. Difference of two LOCA-simulated experiments, USNRC experiment and JAEA experiment was addressed in chapter 2.

1.3. Thesis objectives and organizations

Zircaloy cladding can be failed during loss of coolant accident. To prevent cladding failure and severe accident, LOCA ECCS criteria were established. Two different experiments, LOCA post quench ductility test (U.S.NRC), and thermal shock fracture test (JAEA) was done to supply the experimental data to establish such criteria. For as received cladding, each experiments derived same conclusion, that peak cladding temperature should not exceed 1204℃ and equivalent cladding reacted should not exceed 17%. But for the high-burnup cladding, two experiments got different results. U.S.NRC experiment showed elevated limitations of ECR and PCT, with increasing burnup level, and JAEA experiment showed same limitations on ECR and PCT. The reason why those two experimental methods got different result will be addressed in chapter 2, with the details of each experiment.

High-burnup cladding issue has been drawn up, and U.S.NRC draft rule on burnup and PCT/ECR limit will have significant influence on the regulations of western light water reactors. In this circumstance, the details of experimental protocols should be revised to respond with high-burnup cladding issue. In chapter 3, each protocol will be covered one by one to find out the physical meanings of each protocols, and reasons why we should follow or reconsider those manners.

Chapter 2. Comparison between Thermal Shock Fracture and Post-LOCA Ductility Based ECCS Criteria

2.1. Technical base for Thermal shock fracture based and post-LOCA ductility based ECCS criteria

Two different assessment methods, post-LOCA ductility and thermal shock fracture based experiment exist in establishing ECCS criteria. Both experiments perform simulated-LOCA experiment, which is high temperature oxidation and quenching. But they have different perspective in the decision of cladding integrity. Widely used post-LOCA ductility based criteria utilizes ring compression test (RCT) at 135℃ after simulated-LOCA experiment to decide cladding ductility. 135℃ is cladding temperature after reflood(saturated steam temperature for 3.2 bar), therefore the rationale for selecting this temperature is to assess cladding ductility after LOCA. On the other hand, fracture-based criteria utilize rod integral test to determine whether cladding will fracture due to thermal shock during reflood quenching. Notable difference in two methods is that ductility-based criteria focus on cladding integrity after LOCA, while fracture-based criteria focus on thermal shock during LOCA.

Post-LOCA ductility based criteria has a history from atomic energy committee (AEC) 1973 rule making hearing. Hobson has conducted high temperature oxidation and ring compression test at various temperatures (figure 2-1) and found ductile ECR and PCT limit (figure 2-2.). Hobson judged the ductility of the cladding by the fracture shape of a cladding. If cladding is not fractured during RCT, it is judged as totally ductile.

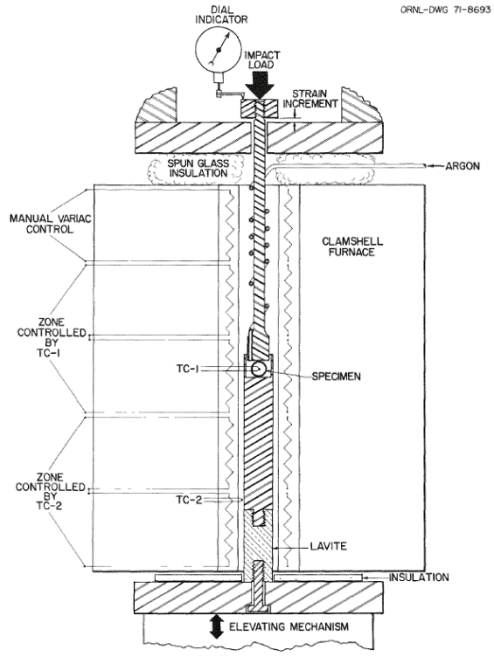

Figure 2-1. Hobson's RCT facility

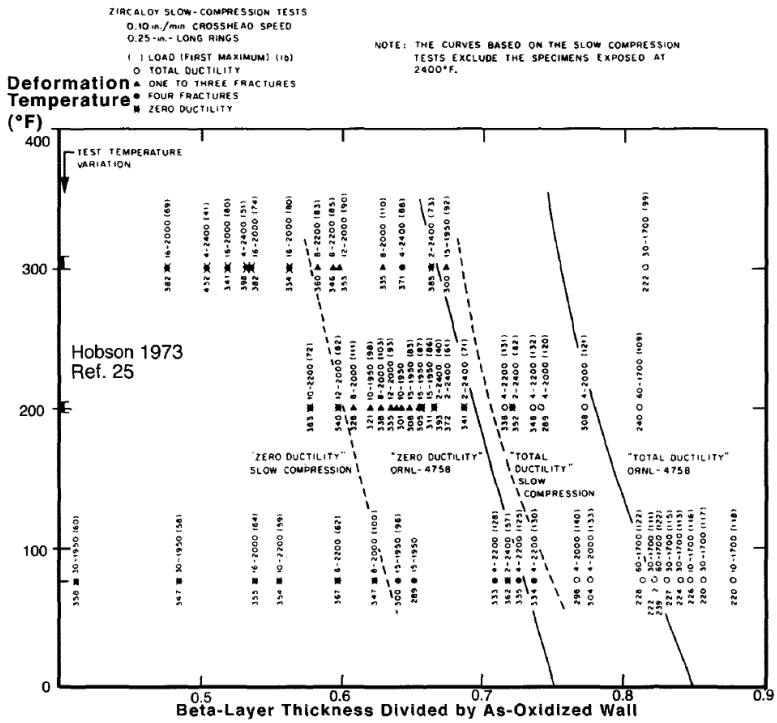

Figure 2-2. Embrittlement limit derived from Hobson's experiment.

Thermal shock fracture based experiment was done at 1983, Uetsuka in JAEA. He used long cladding compared to Hobson's experiment, and restrained bottom and top part of the cladding with load cell (fig 2-3). Fixing the cladding was done to imitate the friction between cladding and spacer grid. By this, he measured thermal shock stress during quench and fracture load.

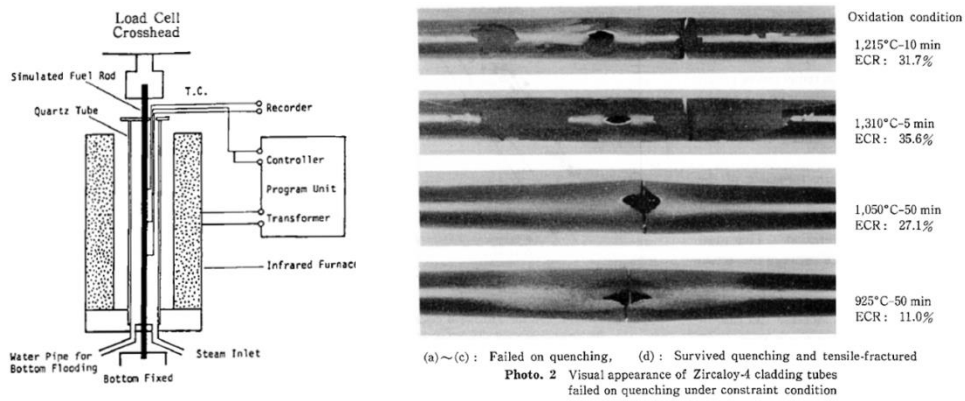

Figure 2-3. Uetsuka's LOCA facility and fracture shape after integral testing

Temperature transient during the experiment was done in the same manner with what Hobson did. Cladding experience temperature ramp, and isothermal oxidation, and quenched. During quenching process, load is imposed to the cladding by the thermal shock and contraction of the cladding (fig. 2-4). If cladding survives during quenching, cladding is judged as maintaining its integrity.

As a result, Uetsuka got ~40% ECR limit for unrestrained conditions, and ~20% ECR limit for fully restrained condition, at 1200℃(fig. 2-5). Japan established 1200℃, 15% ECR criteria, with some additional margin.

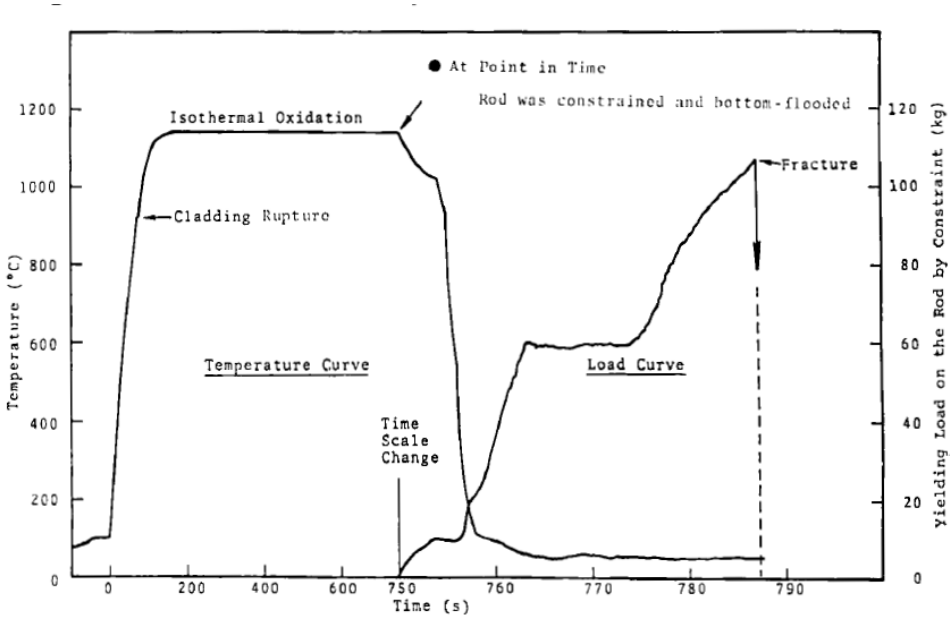

Figure 2-4. Temperature history and load curve in Uetsuka's experiment

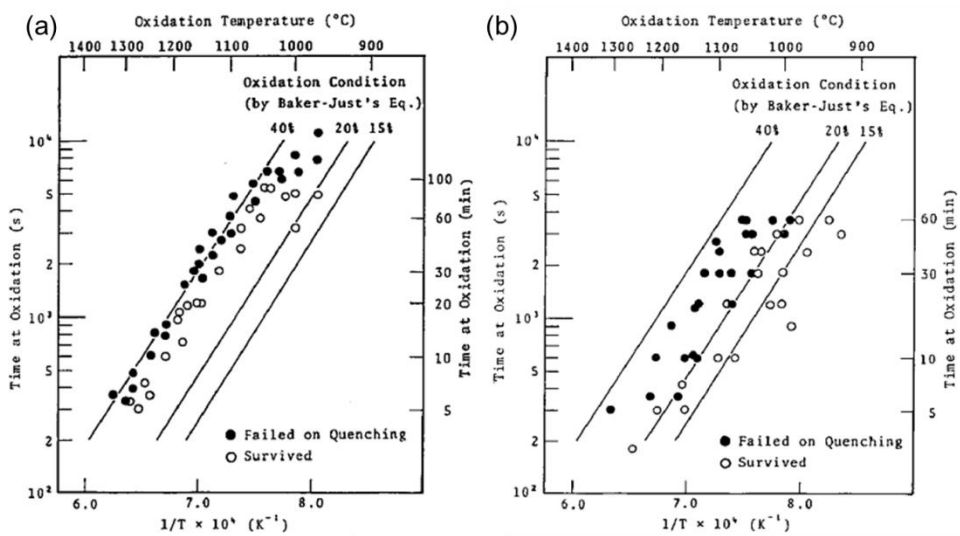

Figure 2-5. Ductility limit for thermal shock fracture based experiment. (a) unrestrained condition, (b) fully restrained condition

When the experiments were conducted with fresh, as-received fuel claddings, both methods draw similar ECR and PCT limit, which is ECR 17% (U.S.NRC), 15%(JAEA) and 1204℃(U.S.NRC), 1200℃(JAEA). In high-burnup cladding, two methods draw different results. Ductility-based criteria lowered its ECR and PCT limit with the increase of burnup(fig. 1-4), while thermal shock fracture-based criteria maintained ECR and PCT limit regardless of burnup increase (Fig. 2-6). To find out the reason of the difference between two methods, each method will be thoroughly discussed in this study.

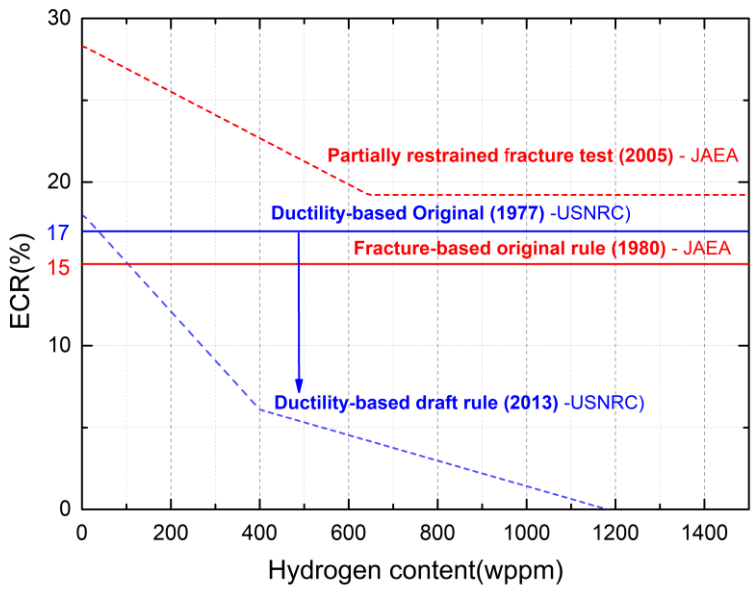

Figure 2-6. Ductility and thermal shock fracture based criteria for high-burnup claddings

2.2. Method

For high-burnup fuels, hydrogen inside the cladding plays important role on determining cladding ductility. If hydrogen is precipitated state, it forms hydride which significantly lowers cladding integrity, while dissolved hydrogen has little influence on cladding integrity. During LOCA transient, hydrogen is either precipitated or dissolved depending on the changing of cladding temperature.

In this study, MARS LOCA simulation, hydrogen precipitation kinetics module, structure analysis module was used to analyze cladding integrity during LOCA(Fig 2-7).

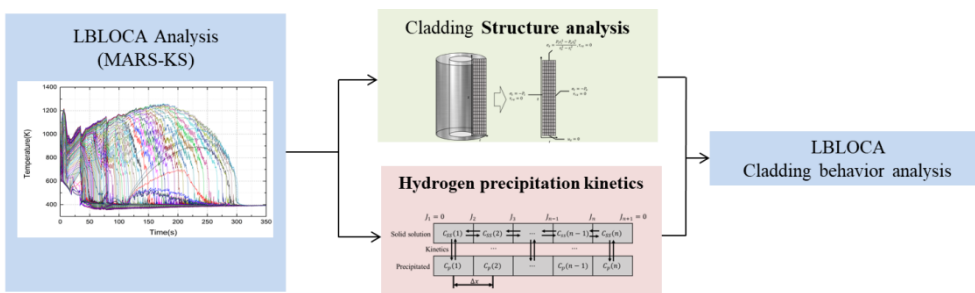

Figure 2-7. Schematic for Code-integrated LOCA analysis

MARS-KS code with KINS-realistic estimate method (KINS-REM) was used to estimate temperature during LOCA. Code input was based on Ulchin(UCN) 3&4, OPR-1000. To get exact and high resolution temperature profile which is needed for structure analysis, cladding heat structure was divided to 99 axial mesh, and 21 radial mesh.

Hydrogen precipitation model is based on Kammenzind's study, and hydrogen precipitation parameter K_p=0.012s^{-1} was acquired from Zanellato's study. Hydrogen kinetics correlation, and terminal solid solution for precipitation (TSSP) correlation is shown below.

$$\frac{dC_{ss}}{dt} = K_p(C_{ss} - TSSp) \quad (2)$$

$$\text{TSSp} = 1.39 * 10^5 \exp(-\frac{34470}{RT}) \quad (3)$$

(C_{ss}: Solid solution hydrogen content

T: Temperature, R: Gas constant)

Structure analysis code is in-house GIFT code using finite difference method (FDM). Calculation accuracy of this code was confirmed by comparing code calculation results and ANSYS calculated results. Stress convergence test was done to increase the credibility of stress analysis (fig. 2-8). Calculation from 30 axial mesh to 6684 axial mesh was done. Stress difference between 1114 axial mesh and 6684 axial mesh was within ~5%, and results with 1114 axial mesh was used to get stress calculation results.

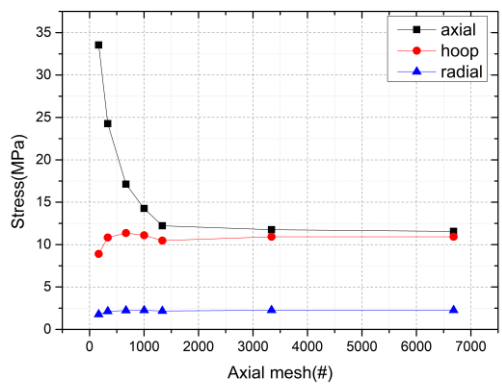

Figure 2-8. Stress convergence results for each direction

2.3. Results and discussions

LOCA analysis in fig. 2-9 shows that peak cladding stress occurred during reflood quenching. And at the timing of peak cladding stress occurrence, (around 200℃) hydrogen is still at dissolved state, because of slow precipitation kinetics. This discordance of peak stress and hydrogen precipitation time occurred generally for all axial position of the cladding. High stress imposed to the cladding at the early moment (~1 sec) was due to the sharp temperature rise and resulting temperature gradient at the beginning of the LOCA.

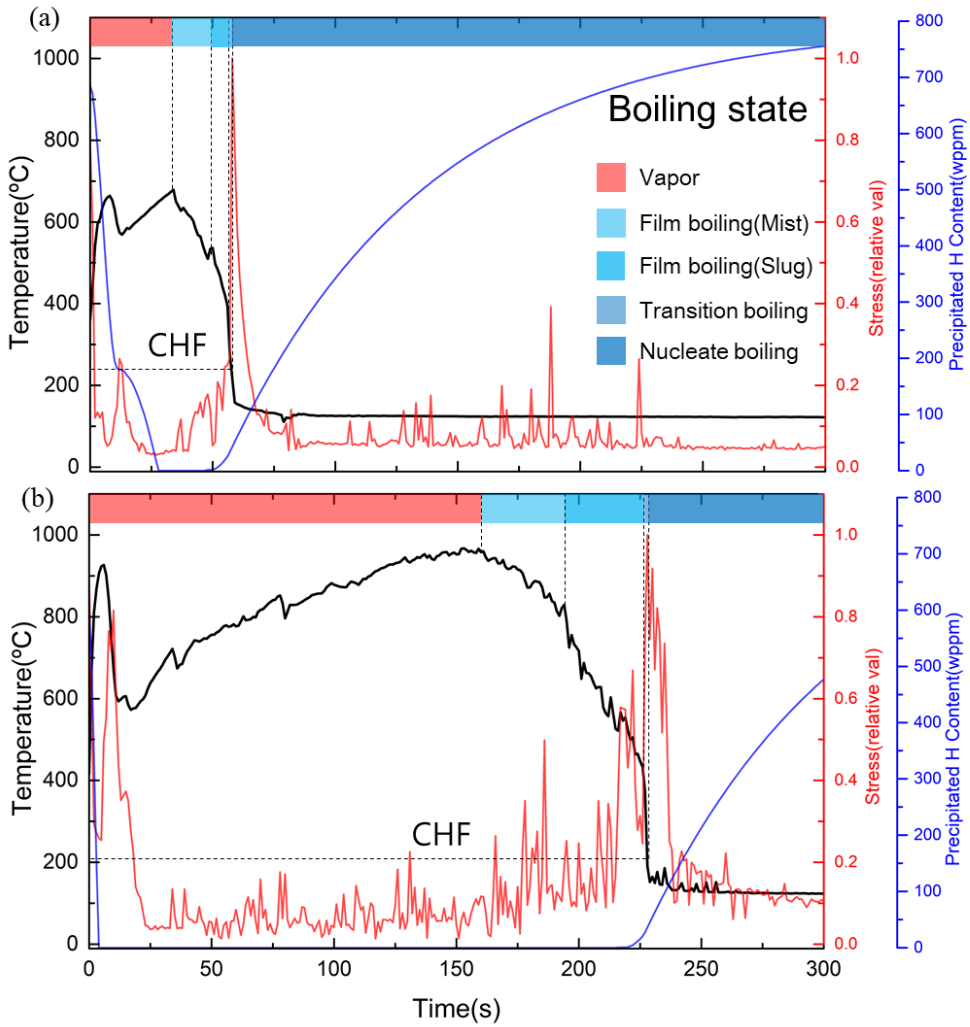

Figure 2-9. LBLOCA analysis of UCN 3&4. (a) Axial location 1.17m, (b) axial location 2.99m

This result explains how fracture-based criteria maintained its ECR limit in high-burnup fuel claddings. It is because of the slow hydrogen kinetics, compared to quick quenching of the cladding during reflood. Since dissolved hydrogen has little influence on the integrity of the cladding, fracture-based criteria could have maintained same ECR limit independent to burnup effect. Nevertheless, for ductility-based criteria, almost all of the hydrogen is in precipitated state (TSSp = 5.3wppm for 135℃). Precipitated hydrogen forms hydride, which severely deteriorates cladding integrity. This resulted in lowering ECR limit for ductility-based criteria.

Cladding located at 1.17m gets thermal shock at ~50s, while cladding at 2.99m gets thermal shock at ~230s. And at the time of ~230s, stress is imposed to the cladding at 1.17m due to the thermal shock of upper part. And at that moment, most of hydrogen is in precipitated at 1.17m. This implies that fracture can occur even after the time cladding get thermal shock, due to the stress propagation from different part of the cladding.

Discrepancy between ductility-based and fracture-based ECCS criteria was explained. During LOCA trainsient, reflood quenching and thermal shock occurs so rapidly that slow hydrogen precipitation does not occur until the end of quenching. As a result, fracture-based ECCS criteria maintained same ECR level for high-burnup claddings.

2.4. Conclusion

Discrepancy between ductility-based and fracture-based ECCS criteria was explained. During LOCA trainsient, reflood quenching and thermal shock occurs rapidly that slow hydrogen precipitation does not occur until the end of quenching. As a result, cladding integrity is maintained during quenching, and fracture-based ECCS criteria maintained same ECR level for high-burnup claddings.

On the other hand, ductility-based criteria is based on ring compression test in 135°C, which is a temperature after the termination of LOCA. In that condition, cladding is embrittled due to the precipitation of hydrogen. As a consequence, ductility-based ECCS criteria could not maintain its embrittlement ECR level for high-burnup claddings.

Both regulations have reasonable background for selecting which point of LOCA they want to address. JAEA selected thermal shock during quench, and U.S. NRC chose the termination after LOCA. It is worth noting that these differences in perspective have caused a big difference in the results.

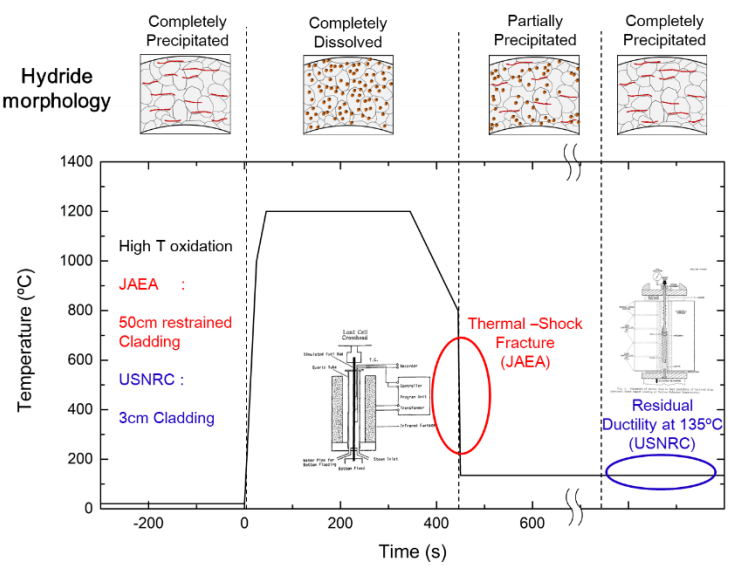

Figure 2-10. JAEA and U.S. NRC LOCA experiment analysis

Chapter 3. Analyzing protocols of LOCA post-quench ductility experiments.

3.1. Experimental procedures for post-quench ductility based criteria

Regulatory guide published by U.S.NRC suggests protocols for establishing LOCA ECCS criteria. Those protocols can be divided into four steps. First step is sample preparation, second is LOCA-simulated experiments, third is sample cutting and RCT, and last is RCT analysis, as shown in fig. 3-1.

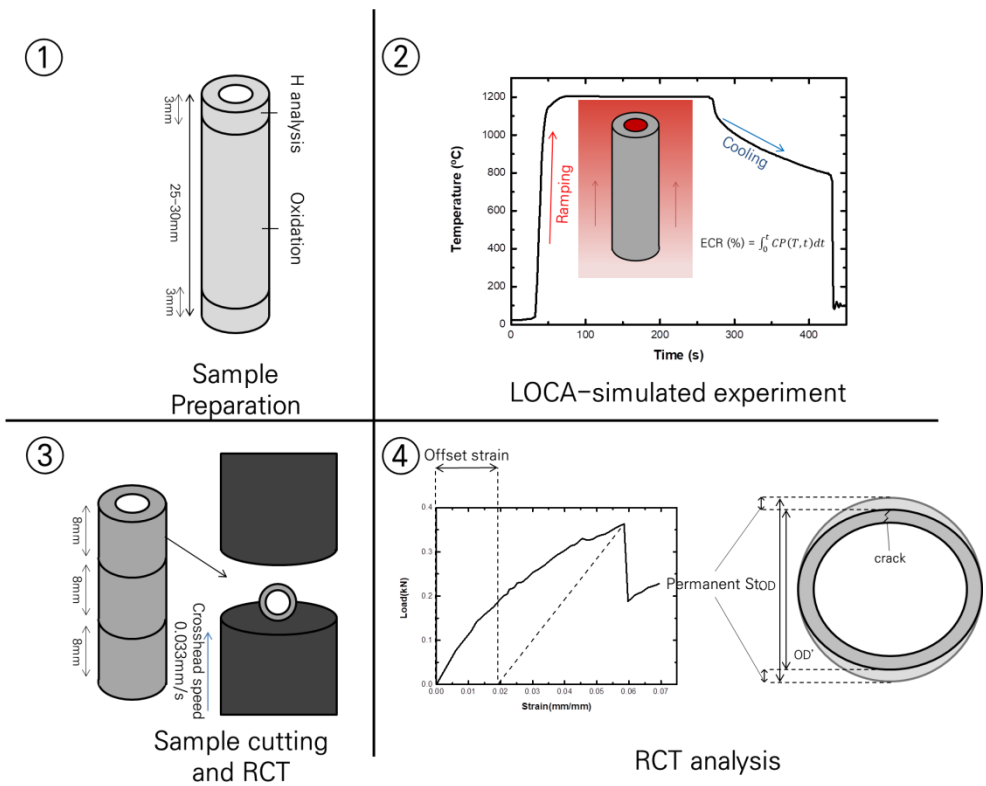

Figure 3-1. Experimental protocol suggested in U.S.NRC regulatory guide

In the specimen preparation stage, hydrogen is injected into the Zircaloy cladding. Hydrogen content analysis of the hydrogen-injected cladding was conducted in two points near to the specimen which will be conducted LOCA experiment. If the results of the hydrogen analysis in the two places show a difference within ±10%, it can be determined that hydrogen is injected uniformly. Thereafter, the specimen was washed and the cladding tube is cut ito 25-30 mm near the site where the hydrogen content was measured. Thickness, outer diameter, and mass of the cladding tube

are measured.

High temperature oxidation experiment is conducted after accurately measuring the temperature of the specimen by the temperature benchmark. The specimen is placed inside the furnace, heated to 1000°C at a heating rate of 30°C/s or more, then heated to 1204°C at a rate of 2°C-3°C/s. After oxidation progresses to the target CP-ECR at 1204°C, it is cooled to 800°C at a cooling rate of 2°C/s or higher rate, and quenched using quenching water(or quenched directly at 1204°C) . After the experiment, thickness, outer diameter, and mass of the cladding tube is measured again and compared with the value before the experiment.

Ring compression test is carried out by cutting the oxidized 25-30 mm specimen into three 7-10 mm specimens. The crosshead speed is 0.033 mm/s, and the temperature of the specimen is 135°C, which is the reactor core temperature after the termination of LOCA. The two key indicators for the RCT are plastic strain and offset strain, which can be measured only when the specimen is not split into two pieces and is cracked thinly. Plastic strain is calculated by the difference between the outer diameters before and after the RCT is devided by the outer diameter before high temperature oxidation. Offset strain is calculated with the intersection with the x-axis by applying the slope at the point of fracture using the strain-load graph.

There are two methods for evaluating ductility and presenting oxidation limits. The first method uses the average offset strain or the permanent strain. Results of the RCT of three specimens (cut from 25-30mm specimen)with the same hydrogen content and the same ECR, are combined into one specimen group. Each specimen group should be set to have an interval of 1% ECR.

1) If the average of the three permanent strains obtained by the loop-axes test of the three specimens is greater than 1%, or the avereage of the offset strain is greater than 1.41+0.1082*ECR, the specimen group is determined to be a "ductile" specimen group.

2) Even if 1) is passed, if the offset strain of at least one specimen is 2% or less or permanent strain 0.8% or less, the specimen group is judged as a "transitional" specimen group.

3) If the average offset strain or average permanent strain is determined to brittle, the specimen group is determined to be a "brittle" specimen group.

4) Among the various specimen groups obtained in this way, the two specimen groups with similar hydrogen contents and different ECR were compared. If the difference in oxidation between the ductile specimen group and the brittle specimen group is 2%, or if the difference in oxidation between the transitional specimen group and the ductile specimen group is 1%, the intersection point of the straight line following the two specimen groups is the oxidation limit at that hydrogen content. The method is illustrated in fig. 3-2 (a).

The second method use curve fit of the offset strain or the permanent strain. And collect the results of the RCT at different ECRs (interval within 1%) with the same hydrogen content, and display them in an ECR-offset strain or oxidation-permanent strain graph. By the curve fitting of the plotted points using a linear or exponential function, the intersection point between the graph obtained and the offset strain reference(from RG 1.223) or the permanent strain 1% line is obtained to obtain the oxidation limit. This method is illustrated in Fig. 3-2 (b).

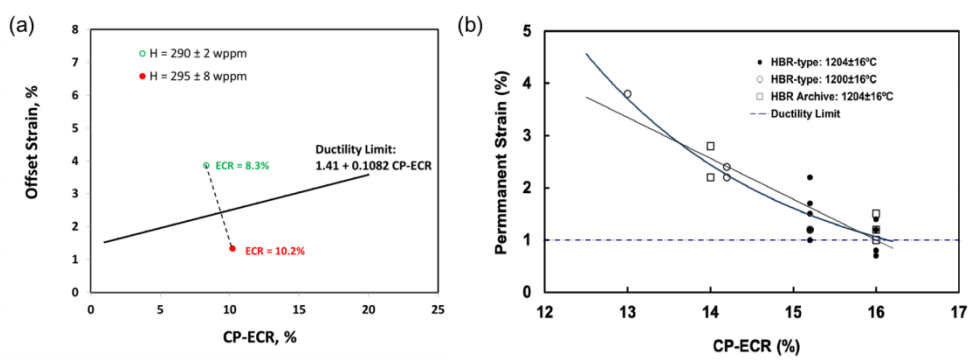

Figure 3-2. Two different methods to analyze RCT results and derive ECR limit.

There are some key experimental conditions in regulatory guide. For LOCA simulation experiment, cooling rate (2°C/s or higher), quenching temperature (800°C or 1200°C), quenching water temperature (not presented above) is important. In RCT, specimen length, crosshead speed, RCT temperatures are important. Each condition will be reviewed one by one to show reason of their significance, especially for high-burnup claddings.

To surrogate high burnup effect of the cladding, pre-hydrided cladding was used in this study. Gaseous charging facility in fig. 3-3 is used to charge hydrogen into the cladding. Furnace temperature during Hydrogen charging was 400℃, and heat treatment was done at 400℃ for 24 hours after hydrogen charging, to make homogeneous distribution of the hydrogen inside the cladding. Resulted hydrogen concentration in cladding ranged from 10wppm ~ 1100wppm.

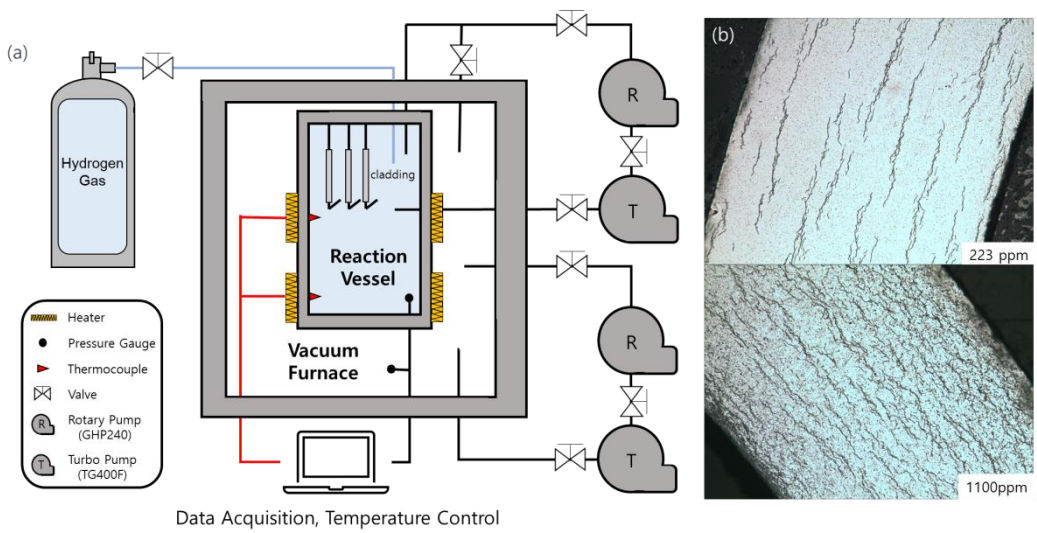

Figure 3-3. (a) Hydrogen charging apparatus, (b) hydride morphology of ZIRLO cladding (223wppm, 1101wppm) captured with optical microscopy

High temperature oxidation and quench test was performed with LOCA facility described in fig. 3-4. Validation of facility was done in previous paper, comparing

oxidation results with Cathcart-Pawel (CP) correlation and TRANOX code, and weight gain results.

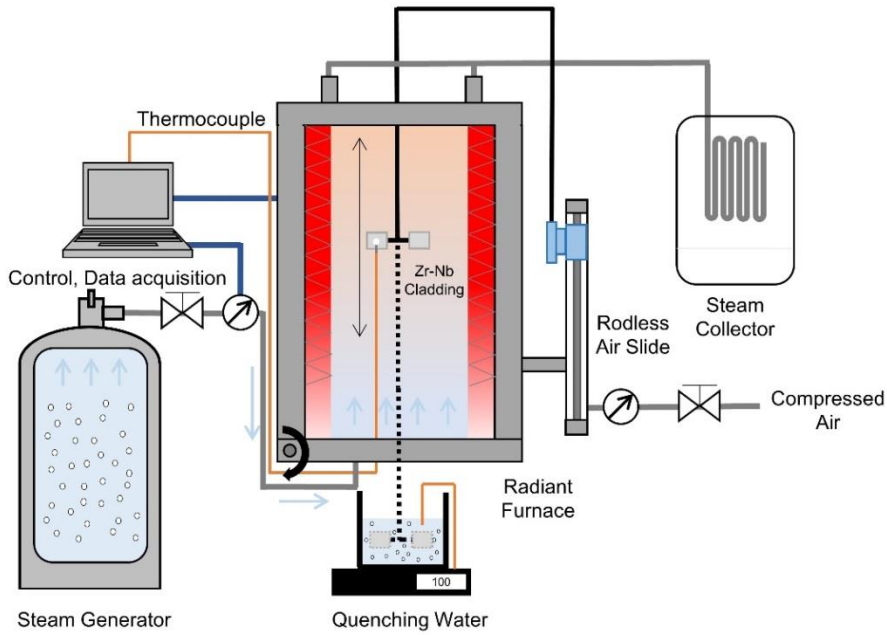

Figure 3-4. Schemetic of LOCA apparatus

In the experiment, 30mm cladding specimen was hanged on specimen holder, and oxidized in furnace. Temperature of the specimen was measured with K-type thermocouple attatched to the specimen with ceramic bond.

3.2. Cooling rate and quenching temperature

Among the key test conditions that are known to affect post-LOCA mechanical behavior, pre-quenching cooling rate has been considered as one of the most complicated effects. Investigation by CEA revealed slower pre-quenching cooling rate of pre-hydrided specimen increases post-LOCA cladding ductility due to the partitioning of alloying elements, and formation of morphologically coarse hydrides. Yet, the applied pre-quenching cooling rate of the CEA's study was ~0.5ºC/s which is considered substantially slower than the actual pre-quenching cooling rate (1 ºC/s ~7 ºC/s). U.S NRC's investigation used the pre-quenching cooling rate of 10ºC/s, which is considered closer to the actual pre-quenching cooling rate, but is still slightly greater than the actual range. An investigation was conducted to compare the post-LOCA ductility assessment of CEA and U.S NRC. The study concluded that difference between two institutions' results were primarily due to different cooling rates, highlighting the important influence of pre-quenching cooling rate on post-LOCA ductility assessment.

Nevertheless, the mechanism of the pre-quenching cooling effect is still controversial and needs further investigation. In addition, the comparison between CEA and U.S NRC was done with pre-quenching cooling rates (U.S NRC: 10ºC/s, CEA: 0.5ºC/s) with limited relevance to realistic LOCA cooling rate range (1 ºC/s ~7 ºC/s). Hence this study aims at exploring the effect of pre-quenching cooling rate on post-LOCA cladding ductility of both pre-hydrided and as-received (hydride-free) cladding materials to revisit its regulatory implications.

Cold work stress-relieved Zr-Nb cladding were used for experiments and their compositions are summarized in **Table 1**. The ID and OD of both cladding are 8.36mm and 9.5mm, respectively.

Table 3-1. Composition of Zr-Nb cladding

	O(wt.%)	Nb(wt.%)	Sn(wt.%)	Zr
Zr-Nb alloy	0.1-0.16	0.8-1.4	0.9-1.3	Bal.

Applied specimen temperature history during oxidation test is shown in Fig 3-5. Slided to the central region of the radian furnace by the rodless air slide upon the initiation of the experiment, specimen is heated at ramping rate of ~40℃/s to the target temperature. Once target temperature is reached, specimen temperature was held constant for periods of time, undergoing isothermal steam oxidation. After the isothermal oxidation, specimens underwent four different cooling modes:

① Directly quenched into boiling water (i.e., 1200°C specimen dropped into pool of boiling water)

② Cooled by Ar gas at rate of 2.5℃/s to 800℃ in the furnace, and then quenched to boiling water

③ Cooled by Ar gas at rate of 0.5℃/s to 800℃ in the furnace, and then quenched to boiling water

④ Cooled by Ar gas at rate of 0.5℃/s to ambient temperature (~25℃ in the furnace) (slow cooled, hereinafter).

The facility was designed to introduce Ar gas into the test section when necessary. Ar gas was able to prevent oxidation during the cooling periods. The tested cooling rates were chosen in compliance with previously tested cooling rates of U.S NRC and CEA for their ECCS rule making. Cooling modes of ①~④ are illustrated in Fig. 3. ECRs of post-LOCA specimens were analyzed by measuring their weight gains and using them in (4). In the meantime, CP correlation ECRs were calculated by (5) using the measured temperature transience of the test.

$$ECR = Wg/(\rho_z h_r) \quad (4)$$

where Wg is weight gain, ρ_z is density of zirconium in g/cm^3, and h_r is thickness in cm

$$Wg = 0.602\exp(-1.005 \times 10^4 T)t^{1/2} \quad (5)$$

where T is temperature in K, and t is time in s

For variable temperature, (5) can be integrated over time period of interest from 0 to t as follows:

$$(\mathrm{Wg})^2 = 0.362\int_0^t exp(\text{-}20100/\mathrm{T})\ \mathrm{dt} \quad (6)$$

After oxidation, the 30mm specimens were cut to three segments of 8mm height and underwent Ring Compression Test was conducted at 135°C. The load-displacement curve of RCT was used to obtain offset strain, and displacement energy density (DED – J). The entire test procedures including sample preparation (i.e., size), steam oxidation, water quenching, and ring compression tests were conducted in compliance with the U.S NRC's reference conditions and protocols outlined in its regulatory guidelines.

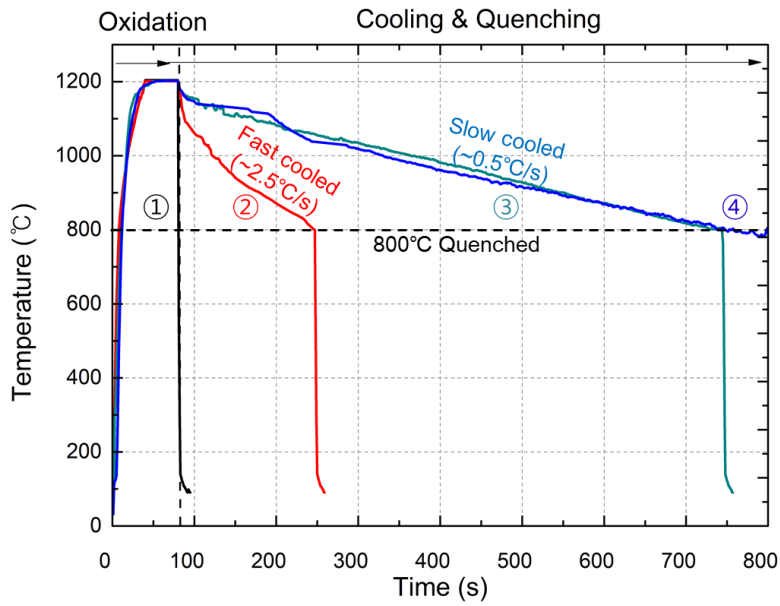

Figure 3-5. Four different tested cooling modes and corresponding temperature history (Note that temperature history of ④ Cooled by Ar gas at rate of 0.5℃/s to ambient temperature is truncated for its extended scale)

Quantification of hydrogen content is an important in reducing the experimental uncertainty. In this study, hydrogen content of a tested specimen was assessed in two cross-checking steps, which is demonstrated in Fig. 3-6. Firstly, once hydrogen is

charged and cut to 30mm height specimen, the cut segments of the top and bottom of the 30mm specimen was collected and their hydrogen contents are measured. For both the top and bottom segments, hydrogen contents of three different azimuthal locations were measured, giving total six measurements for both ends. This is the first stage of hydrogen content measurement. Then, 30mm specimen was cut to three 8mm specimens for RCT tests after the completion of LOCA test (steam oxidation and water quenching). One of the three post-RCT specimens was tested for hydrogen measurement. Specifically, three segments of one of the three post-RCT specimens were tested for hydrogen measurements for the second stage, which is then compared against the previously obtained hydrogen measurements done in the first stage. The presented results consistently gave the average hydrogen content difference less than 30wppm between the first and second stage of hydrogen measurements, demonstrating that the hydrogen distribution is uniform in the tested 30mm specimen thereby validating the use of a single hydrogen content for the three 8mm specimens.

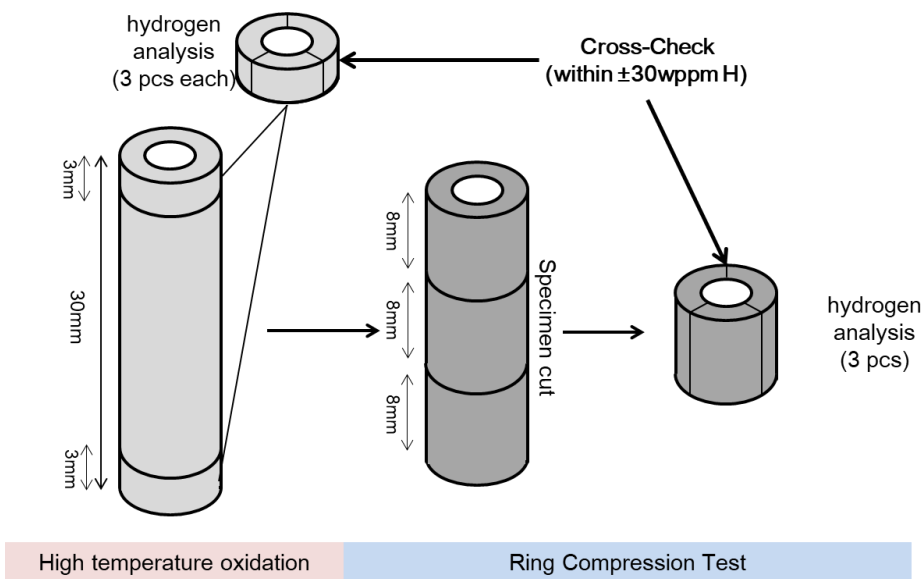

Figure 3-6. Demonstration for Hydrogen content measurement

High temperature oxidation and RCT experiment was conducted using as-received and pre-hydrided specimen (160 wppm). Both specimens were oxidized to ~8% ECR. 8% ECR was chosen because it is near the ductile-brittle boundary of Zircaloy specimens based on the offset strain criterion of the U. S NRC [10]. RCT results of four different cooling conditions are shown in Fig. 3-7 and their key parameters are summarized in Table 3-2. As can be noted in Fig. 3-7 (a), higher cooling rates (①> ②>③>④) lead to higher cladding ductility for as-received specimens. This is also evidenced by the offset strain analysis. As opposed to this trend, for pre-hydrided specimen (160 wppm) the higher cooling rate result in greater cladding embrittlement. This result clearly demonstrates that the effect of cooling rate on mechanical behavior of post-LOCA specimen distinctively changes with respect to hydrogen content.

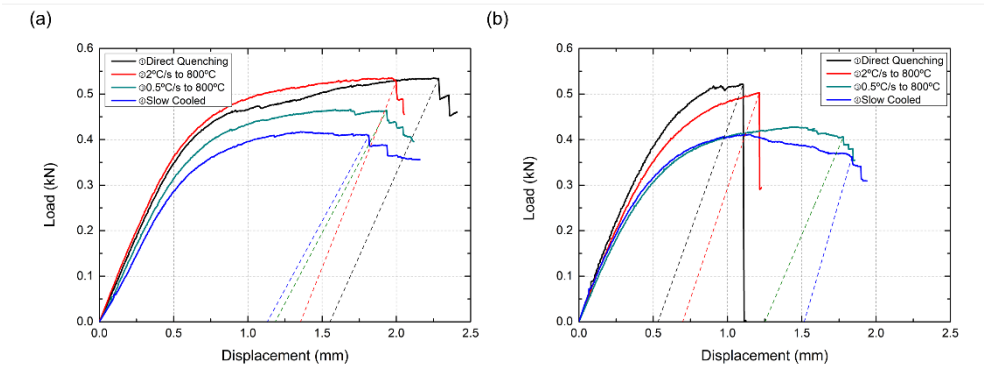

Figure 3-7. 4 Load-Displacement curve of Different temperature history (a) as-received cladding (b) pre-hydrided cladding (160 wppm)

Table 3-2. High temperature oxidation and RCT results for different cooling rate using pre-hydrided 160wppm and as-received Zr-Nb specimen.

Cooling conditions	①		②		③		④	
Quenching Temp	1200℃		800℃		800℃		No Quench	
Cooling rate	No Cooling		2℃/s		0.5℃/s		< 0.5/s	
CP-ECR	8.0%		7.8%		8.1%		8.2%	
Measured-ECR	8.0%		7.7%		8.1%		8.2%	
	Pre-hydrided	As-received	Pre-hydrided	As-received	Pre-hydrided	As-received	Pre-hydrided	As-received
Av. Offset strain(%)	7.7	16.0	8.7	13.6	13.0	13.1	15.1	10.2
Displacement Energy Density(J)	1.30	3.76	1.52	2.81	1.94	2.56	2.13	1.75
Fracture Load(kN)	0.49	0.54	0.51	0.53	0.40	0.46	0.37	0.41

EBSD analyses were conducted to investigate the mesoscale mechanism behind the different cooling rate effect with hydrogen. Fig. 3-8 shows that the grains of post-LOCA specimens are larger for lower cooling rates. Such that direct cooling (①: quenching from 1200°C to boiling water) exhibits the smallest average grain size (average 7.0μm) whereas slow cooling (④: cooled by Ar gas at rate of 0.5℃/s to ambient temperature) exhibits the largest average grain size (average 82.8μm). This result is quite understandable; increased exposure time to high temperature associated with slow cooling allows longer period for grain growth. The dramatic change in grain size makes the material lose its engineered texture (Fig. 3-9). This result is indeed consistent with a previous study that investigated the dynamic grain growth of Zircaloy in high temperature (1100 – 1300 °C) steam oxidation

environments [7]. The dramatic grain growth of Zircaloy subjected to high temperature steam oxidation (>1000ºC) is known to deteriorate material's ductility. This is commonly observed in HCP materials such as Ti and Zr where deformation is contributed by twinning [17-18]. As a consequence, increasing cooling rate shortens grain growth time, thereby helping to suppress ductility degradation. In addition, it is possible to conjecture that extended high temperature exposure with slow cooling may promote diffusion of oxygen in Zircaloy matrix, resulting in the increase of oxygen concentration in the ductility-carrying prior-β phase. This effect also acts to deteriorate cladding ductility.

A past investigation demonstrated that slower cooling promotes partitioning of alloying elements, resulting in the reduced concentration of alloying elements and even oxygen in prior-β phase via $\beta \rightarrow \alpha$ transition [12-13]. This is known to increase ductility of prior-β phase. Nevertheless, this effect is not considered to be not predominant as slow cooing rate of as-received specimen reduced cladding ductility. This implies that the grain size increase with slow cooling is a more dominant effect.

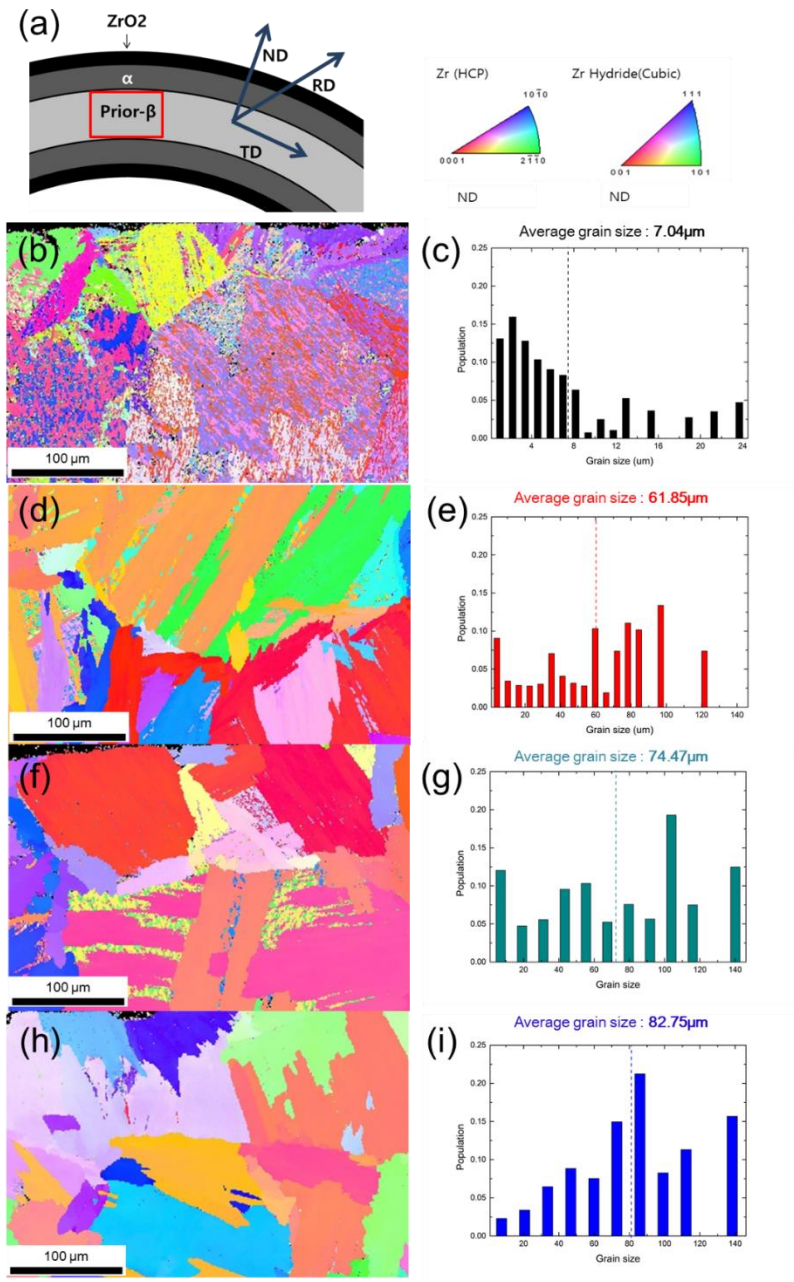

Figure 3-8. EBSD analysis results (Inverse Pole Figure(IPF), grain size distribution) for four different cooling conditions. (a) schematic for cladding microstructure, (b),(c) Directly quenched into boiling water, (d), (e) Cooled by Ar gas at rate of 2.5℃/s to 800℃, (d), (h) Cooled by Ar gas at rate of 0.5℃/s to 800℃, (e), (i) Cooled by Ar gas at rate of 0.5℃/s to ambient temperature.

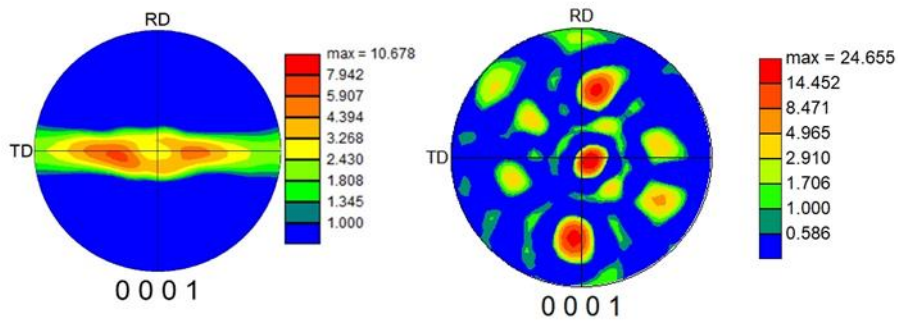

Figure 3-9. Pole figure of (a) as-received Zr-Nb specimen (typical tilted radial basal pole texture), (b) post-LOCA Zr-Nb specimen oxidized to 8% ECR at 1200℃

It is important to note that hydrided specimen, however, exhibits increased cladding ductility even in the presence of the aforementioned adverse effect of larger grain sizes due to slower cooling rate. This makes us investigate effect of cooling rate on resulting hydride morphologies of post-LOCA specimen. Fig. 3-10 shows hydride (red) morphologies in prior-β phase of post-LOCA zircaloy for the tested cooling rates. As can be noted, the faster cooling (①>②>③>④) lead to smaller and less connected hydride morphologies because of reduced diffusion period for phase transformation. For the direct quenching case (①), nano hydride morphology is observed, implying that hydride precipitation occurred without appreciable hydrogen diffusion. On the contrary, the slow cooling case (④) exhibits integranular hydride precipitation which is known as a result of diffusional phase transformation. Both nano hydrides and connected intergranular hydrides are known to deteriorate cladding ductility. However, a past study demonstrated pronounced decrease of dislocation mobility with nano hydrides in Zircaloy. Hence, it is considered that the pronounced diffusionless nano hydride formation with fast cooling rate adversely affect resulting cladding ductility. This effect is considered to outweigh the benefit of the smaller grainsize, thereby resulting in the net effect of ductility decrease with increasing cooling rate.

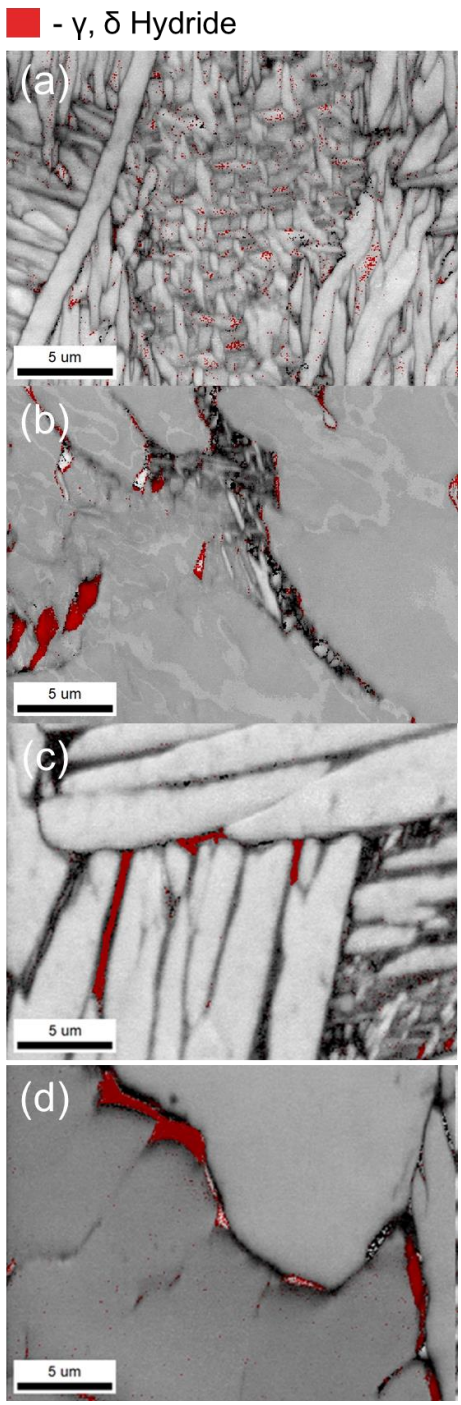

Figure 3-10. Hydride morphology for four different cooling conditions (a) Directly quenched into boiling water, (b) Cooled by Ar gas at rate of 2.5℃/s to 800℃, (c) Cooled by Ar gas at rate of 0.5℃/s to 800℃, (d) Cooled by Ar gas at rate of 0.5℃/s to ambient temperature

Kikuchi pattern analysis was done to increase the credibility of EBSD phase analysis for hydrides. γ-hydride and δ-hydride were both appeared in the EBSD pattern analysis shown in Fig. 3-11 (a). A past study showed that fast cooling rate over 10℃/s can result in γ-hydride, and slow cooling rate less than 2℃/s. In this study, both γ-hydride(yellow) and δ-hydride(blue) were observed to coexist.

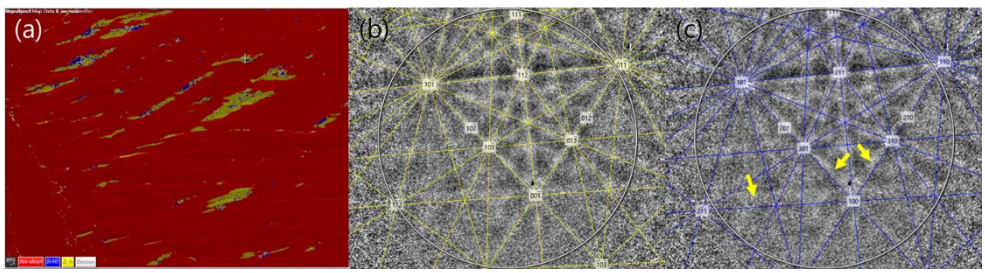

Figure 3-11. (a) Phase analysis and kikuchi pattern analysis for (b) γ-hydride and (c) δ-hydride (EBSD figure for cooling mode ② Cooled by Ar gas at rate of 2.5℃ /s to 800℃ in the furnace, and then quenched to boiling water)

The presented result illuminates the importance of cooling rate on post-LOCA ductility. Even seemingly similar slow cooling rates (0.5 ºC/s and 2.5 ºC/s) yield different post-LOCA ductility resulted by different microstructures. This poses a fundamental issue of standardizing post-LOCA ductility assessment method and condition. During LBLOCA transience, cladding is subjected to a wide range of cooling rate prior to reflood quenching (1.2 ºC/s – 6.4 ºC/s) and quenching temperature (450 ºC - 790 ºC) depending its axial position as demonstrated by MARS simulation, as shown in Fig. 3-12. In today' regulation, reference quenching temperature (800ºC for U.S NRC) and cooling rate (>2.0 ºC/s) are used. However, as can be inferred from this study, different cooling rates above 2.0 ºC/s will result in inconsistent post-LOCA ductility assessment, which may imply a need to further specify the cooling rate. On the other hand, it is questionable if specification of reference cooling rate is even appropriate. If it has to be done, a careful analysis needs to be done to explore the cooling rate and quench temperature of the most limiting location (i.e., highest ECR). This is a formidable task if it is ever possible. This may naturally lead to a corollary; it calls for a lenient regulatory judgement on

potential difference arising from a plausible range cooling rates and quenching temperatures.

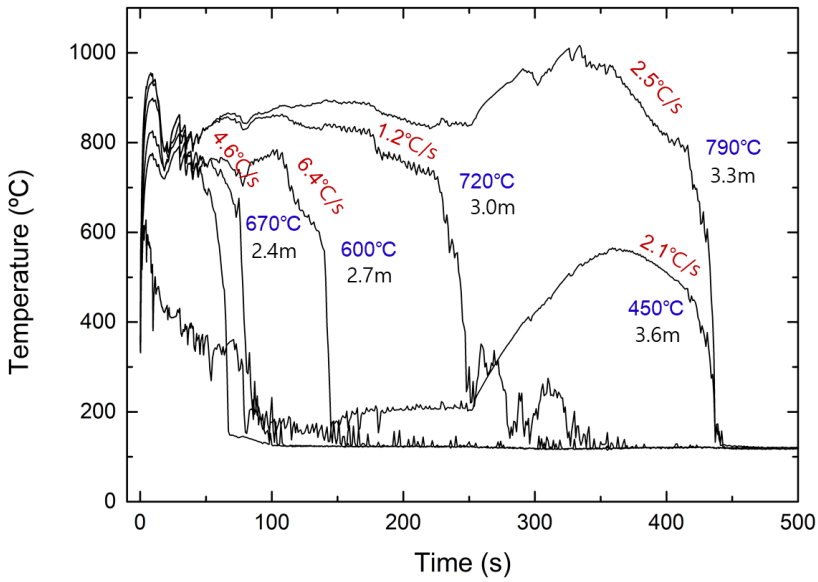

Figure 3-12. Temperature history during LBLOCA. Pre-quenching cooling rate, quench temperature, axial location are shown. (Hottest rod in UCN 3&4, OPR-1000 using MARS-KS code)

Pre-quenching cooling rate	0.5°C/s to air	2°C~0.5°C/s to 800°C	Direct quencing
Grain Size	Large	Intermediate	Small
Hydride Morphology	Continuous hydride	Small hydride	**Nano hydride**
Phase Layer Change (β→α)	Fully changed	Partially changed	Not changed
Alloying Element Precipitation	Fully precipitated	Partially precipited	Not Precipitated

: Ductility decrease

Figure 3-13. Microstructure change with cooling rate

3.3. Quenching water temperature effect

It is important to note that temperature of water bath into which oxidized specimen is quenched has traditionally been overlooked in post-LOCA cladding ductility assessments. Partly due to the lack of attention in the founding experiment, little attention has been made to the water bath temperature effect in subsequent investigations to date. Water bath temperature was unreported in Hobson's work. Recent investigations recorded specimen temperature after bath, specimen temperature varied from 80°C to 100°C dependent to size of the sample. Reflood water during LOCA is saturated water after refilling, this means a gap between the conducted experiments and in-core environments. The water quenching captures rapid cooling and thermal stresses arising from reflood quenching. In the post-LOCA cladding ductility assessments, water bath temperature determines cooling rate. The effect of cooling rate is considered twofold: (1) it may alter the resulting phase characteristics and microstructure; (2) it may affect structural integrity of the brittle phase (α and ZrO_2);

As for the resulting phase characteristics and microstructure, different cooling rates may alter the kinetics of phase transformations upon quenching, thereby changing the characteristics of resulting phases. Holt investigated the microstructure difference due to the cooling rates. From 1050°C to room temperature, cooling rates ranging from 2K/s to 2000K/s were observed. Specimen cooled at 2000K/s showed martensitic microstructure, while specimens cooled at a rate less than 200K/s showed Widmanstätten basket-weave structure with parallel-plates (lamellar). Woo and Tangri showed microstructure difference with oxygen contents of 0.13wt%-0.91wt% and showed that increasing content of oxygen promotes the parallel-plate structure. Measured grain size and lamella thickness has decreased with cooling rate. Microstructure hardness was measured for different cooling rates, and showed that beta-layer hardness increases with cooling rate. Yet, the effects of resulting microstructures under different cooling rates on the cladding's post-LOCA mechanical behavior have not been investigated.

As for the second effect, recent advances on thermal shock fracture studies revealed the importance of heat transfer rate on brittle materials' thermal shock fracture upon water quenching. Chemical Vapor Deposited (CVD) SiC quenched in saturated water (~100ºC) exhibited superior thermal shock tolerance compared to specimens quenched in the room temperature water, owing to the promotion of film boiling that lowers transient temperature gradient within the solid. The observed effect is remarkable as the threshold solid temperature for a crack to propagate was different more than 1000ºC between the saturated and room temperature quenching. Similar observation was made for Al_2O_3 coupons thermal shocked by a room temperature droplet impingement. Al_2O_3 coated with hydrophobic layer which promotes film boiling exhibited superior thermal shock tolerance. These results demonstrate that the brittle phase fracture is tightly coupled to thermal hydraulic behavior of quenching liquid. The importance of the water side heat transfer rate for fuel fracture during LBLOCA was theoretically elaborated by a past study. These past research results illuminate the need to explore the effect of quenching rate on the structural integrity of brittle phases of oxidized Zircaloy and its effect on post-LOCA Zircaloy ductility.

Past study from ANL showed that there is no ductility change for as-received, steam-oxidized sample from 800ºC quenched specimen and air-cooled specimen. For pre-hydrided specimen, ductility increased for slow-cooled specimen compared to quenched specimen due to the mobility of hydrogen below 800°C. Also, another linked study in CEA showed that ductility increasing effect of slow cooling in pre-hydrided specimen is more pronounced in the slow cooling in temperature above 600ºC.

In such a context, this paper aims at systematically exploring the effect of quenching rate on residual ductility of post-LOCA Zircaloy-4. Three different cooling rates associated with distinctively different quenching environments are tested; ambient air cooled (~7ºC/s), boiling water (~400-500ºC/s), room temperature water (~1600-2000ºC/s). Zircaloy steam oxidation, water quenching, and ring compression tests were conducted in compliance with the U.S NRC's experimental procedures and

protocols. With this investigation, this study revisits regulatory implications associated with cooling rates and pre-hydrided high burnup Zircaloy cladding.

As-received and pre-hydrided Zircaloy-4 specimens were used for testing. Zircaloy-4 was pre-hydrided to 765wppm in a hydrogen charging chamber at 400°C to mimic high burnup embrittlement. LOCA experiments consisting of cladding steam oxidation and subsequent cooling (water quenching or air cooling) were conducted for both as-received and pre-hydrided Zircaloy cladding). Cooling rates in 100℃ water and 25℃ water were obtained by the high speed video camera, measuring the time between water quenching and surface bubble disappearance which corresponds to saturated temperature (~100℃). For example, in 100℃ water, it took ~2.5 secs for boiling to disappear upon quenching, giving the cooling rate estimation of 440℃/sec (=1200℃ - 100℃/2.5sec). Resulting cooling rate estimations are ~400-500℃/s in 100℃ water, and ~1600-2000℃/s in 25℃ water. The obtained cooling rate in 100 °C water quenching is in the range of the cooling rates (10 – 700 K/s) in a two phase-fluid above the collapsed water front of bundle tests. Udagawa measured air cooling rate of Zircaloy-4 cooled from 1200 °C to 900 °C, which is 7K/s. And massih measured air cooling at 5mm depth from 1050 °C to 800 °C, which is 3K/s. Since the phase transision of β to α phase occurs in temperature range higher than 800 °C, assuming our cooling rate in air in the range of ~3-7K/s is plausible. RCT was conducted on post-LOCA specimens. Metallographic examinations were conducted using Scanning Electron Microscopy (SEM), Energy-Dispersive Spectroscopy (EDS), and Optical Microscopy (OM). Digital Image Correlation (DIC) was used to measure strain fields of cladding specimen's cross section during RCT. Microhardness of resulting phases was measured. This section discusses details of the conducted experiments.

As-received cold work Zircaloy-4 tubular specimens (OD=9.5 mm and 0.57mm thickness) were cut into 50mm length. Prepared specimens were put into vacuum furnace and 53,000Pa of hydrogen was injected at 400°C. After injecting hydrogen for 4 hours, 24 hours of heat treatment was conducted to homogenize hydrogen distribution in the specimens. As a result of this homogenization, difference in

hydrogen content in the tube was within 10%. Hydrogen concentration was analyzed with ONH-2000. Hydrogen charging of 765±18 wppm shown in Fig.3-14 was achieved and used in this experiment. This amount of hydrogen represents considerably high discharge burnup $\geq 60\mathrm{MWd/kgU}$. The hydrogen charged and as-received Zircaloy-4 specimens were cut to 10mm in length for LOCA and RCT tests.

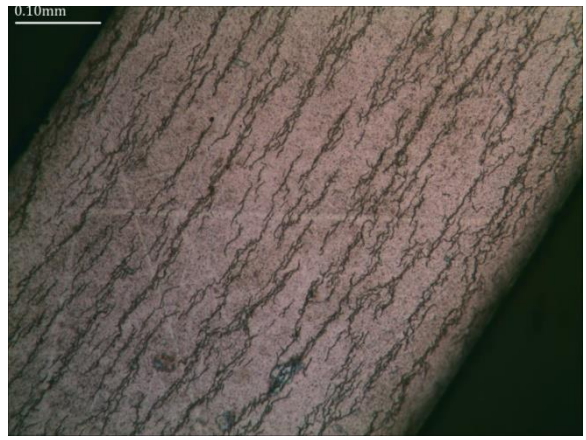

Fig.3-14. Optical microscopy of hydride distribution (765±18 wppm)

Post-LOCA oxygen distribution was measured using EDS. As shown in Fig. 3-15 (a) and (b), no appreciable difference in oxygen distribution was observed between as-received Zircaloy-4 and pre-hydrided (765wppm) Zircaloy-4. Since EDS measurement has limitation on its quality due to surface contamination after polishing, the overall distribution of the oxygen is still similar considering the contamination.

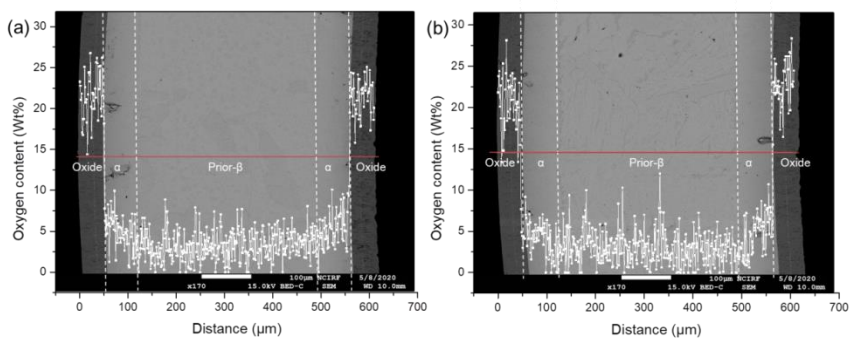

Figure 3-15. EDS Oxygen distribution of ~17% ECR at 1204ºC: (a)As-received, (b) hydrogen charged (765wppm) specimen

Thickness of each phase (oxide, α, and prior-β) was measured at four different locations for each specimen oxidized to 17% ECR at 1204°C. It is notable that the cooling rates have shown limited effect on the thickness of resulting phases (Fig. 3-16 (a) and (b)) for both as-received and pre-hydrided Zircaloy-4, respectively. Since the prior- β phase is the only potentially ductile phase, this result may imply limited effect of cooling rates on mechanical resistantce of the oxidized Zircaloy-4 at a given hydrogen content.

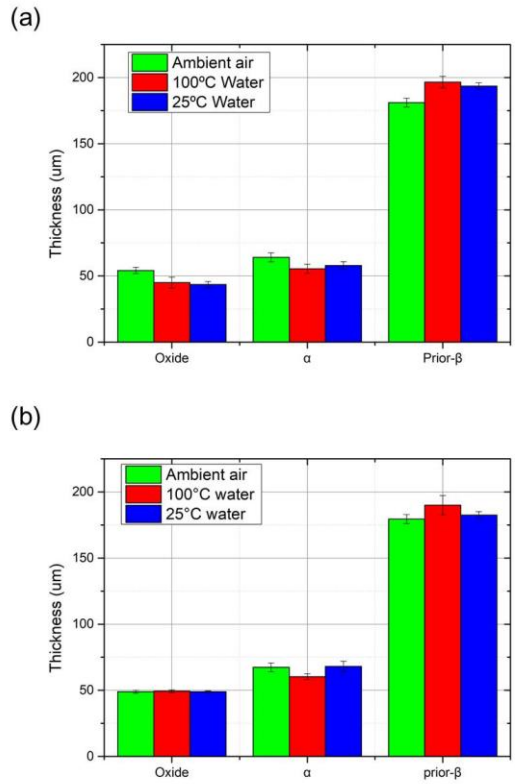

Figure 3-16. Phase layer thickness of specimens oxidized to 17% ECR at 1204°C. (a) As-received, (b) pre-hydrided (765wppm).

Average oxygen content of each phase layer associate with 17% ECR at 1204°C was measured by EDS scanning, and the result is shown in Fig 3-17(a) and (b). Oxygen has a detrimental effect on the residual ductility. As can be noted in Fig 3-15 (a) and (b), no appreciable oxygen content difference is observed for different cooling rates.

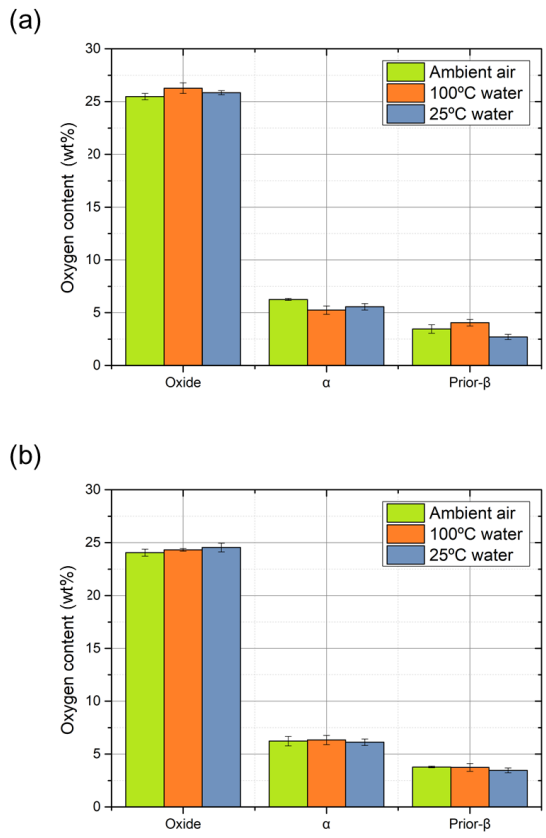

Figure 3-17. Averaged oxygen content of each phase layer of specimens oxidized to 17% ECR at 1204°C. (a) As-received, (b) pre-hydrided (765wppm). Average value of EDS scanning (1000μm^2) is presented.

The β phase formed during high temperature steam oxidation energetically favors to transform into α phase upon cooling below 900°C. All tested cooling rates ranging from ~7 °C /s to 1600-2000°C /s did not allow sufficient time for significant amount of β-to-α phase transformation to occur. This resulted in the 'frozen' high temperature phase snapshot of prior-β, α, oxide phase in ambient temperature. These resulting phases were found to be comparable in terms of average individual phase layer thicknesses and their oxygen content.

Nevertheless, different cooling rates resulted in different microstructures of prior-β phase. Fig.3-18 (a) – (c) show resulting microstructures of prior-β phase for each

cooling condition. While α incursion in prior-β occurred for all tested specimens, it was most pronounced in the air cooled specimen. Extended cooling period with ambient air promotes α incursion in prior-β. The increase of α incursion is considered to decrease homogeneity of the prior-β phase, thereby increasing the statistical variation of RCT behavior (section 3.3). Ambient air cooling resulted in Widmanstätten basket-weave microstructure in the prior-β phase (Fig.3-18 (a)). 100°C water quenching and 25°C water quenching resulted in parallel-plate structure and martensitic structure, respectively. Both Lamellar width and colony size decreased with increase of cooling rate. This result is consistent with past studies on Zircaloy phase transition. Oxygen diffusion is the main mechanism of shaping the lamellar structure. Hence, when cooling rate is higher, this process is limited by decreasing diffusion, resulting in shorter lamellar width.

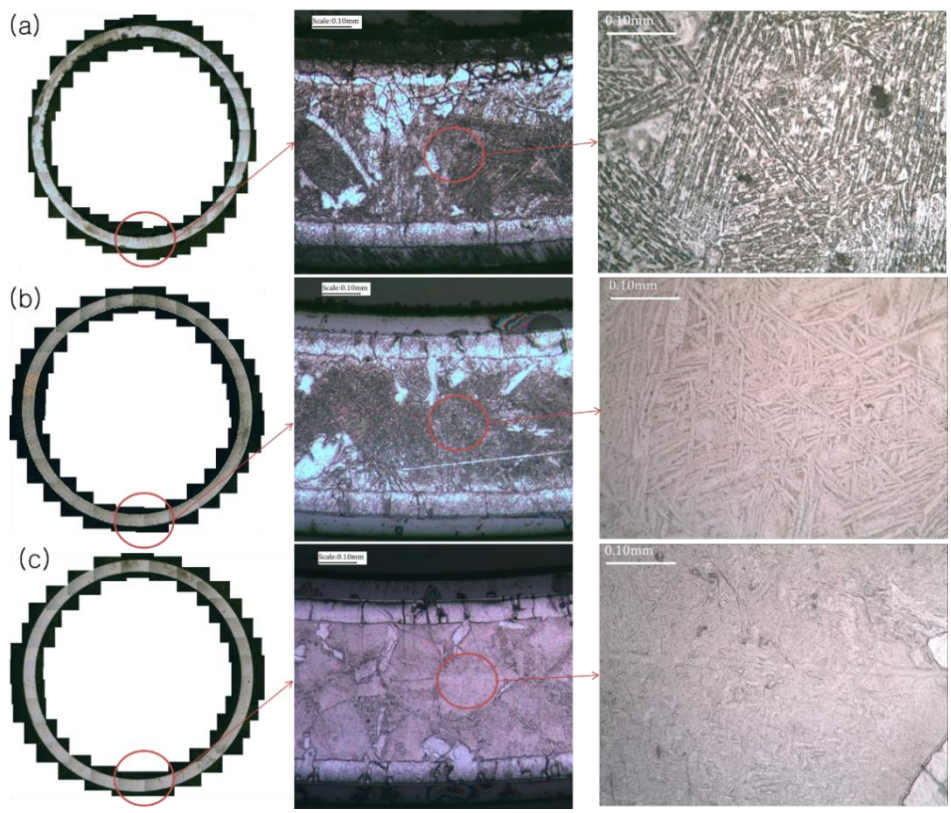

Figure 3-18. Metallographic Analysis of post-LOCA Zircaloy-4 specimens (1204°C and ~17% ECR) (a) ambient air cooled, (b) 100°C water quenched, (c) 25°C water quenched

Consequently, it can be summarized that the tested cooling rates (7 ºC/s to 1600-2000 ºC/s) on Zircaloy-4 steam-oxidized to 17% ECR at 1204ºC:

(1) do not change the average individual phase layer thicknesses;
(2) changing effect on the oxygen contents of individual layers seems to be limited;
(3) affect α incursion in prior-β; and
(4) change microstructure of prior-β phase.

(1) and (2) speak for the possibility of cooling rate insensitivity on cladding residual ductility, whereas (3) and (4) may imply the opposite case. RCT investigation presented in Section 3.3 addresses the effect of these features on residual ductility.

High speed video camera was used to record boiling modes of Zircaloy-4 specimens quenched from 1204ºC at 17%ECR into room temperature water (25ºC) and saturated water (100ºC). As Fig.3-19 (a) and (b) show, saturated water significantly promotes film boiling on surfaces of quenched specimens. At 0.2s, vapor film is covering the specimen in saturated water quenching (Fig. 3-19 (a)) while transition into nucleate boiling is underway in room temperature water quenching (Fig. 3-19 (b)). The enhanced film boiling in saturated water is characterized by thicker vapor film, and lower heat transfer rate compared to highly subcooled boiling. The thermal insulation effect lowers temperature gradients of the solid, thereby reducing thermal stresses associated with differential thermal displacements. Hence the order of thermal stress is 25ºC water quenching, 100ºC water quenching, and ambient air cooling in descending order. Reduced thermal stress is particularly effective in ensuring the structural integrity of brittle materials whose failure mechanism is dictated by local tensile-stress concentration.

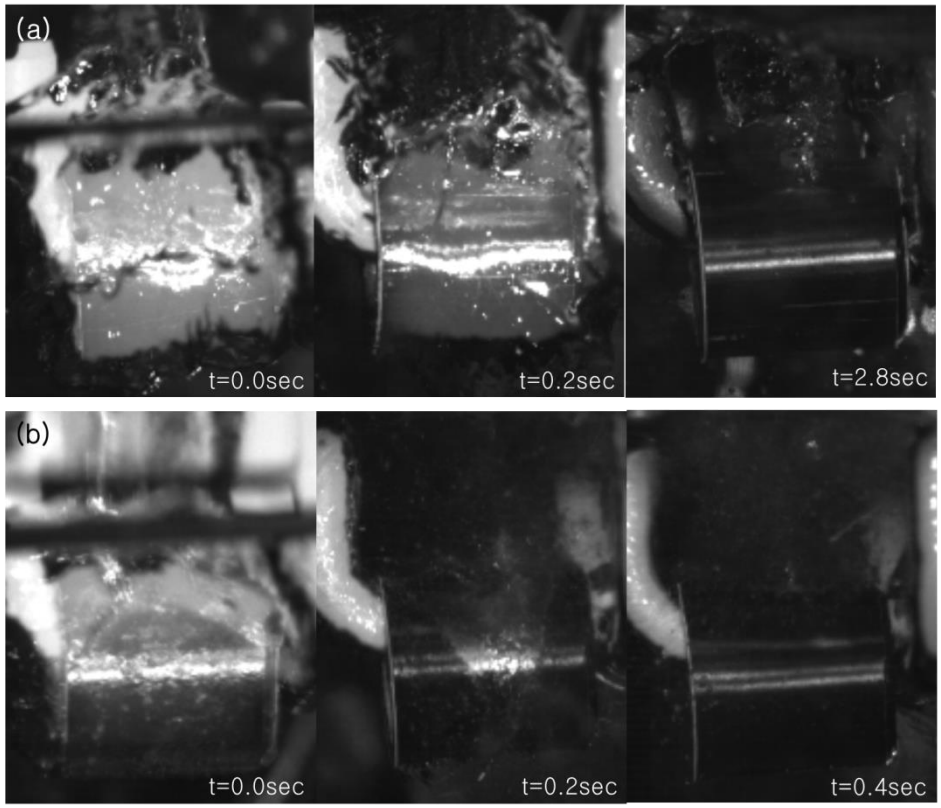

Figure 3-19. Boiling modes of Zircaloy-4 quenched into (a) 100ºC water (saturated) (b) 25 ºC water.

Impact of cooling rate on integrity of resulting phases was investigated by Optical Microscopy (OM), Scanning Electron Microscopy (SEM), and micro-hardness measurements. OM and SEM examinations show no sign of crack development on the specimen surfaces. Vicker's hardness measurements conducted on individual layers in Fig.3-20 (a) showed no marked differences with respect to cooling rates (Fig.3-20 (b) and (c)). Some sign of hardness reduction was observed for the oxide scale of as-received Zircaloy-4 quenched into 25ºC water (the highest cooling rate), as shown Fig.3-20 (b). This may be partly due to internal crack development. As compared to as-received Zircaloy-4, pre-hydrided specimens exhibit different prior-β phase hardness for different cooling rates. Yet, no correlation is identified between the cooling rates and hardness of prior-β phase for the pre-hydrided specimens, implying that the difference may be due to the statistical nature of mechanical behavior of brittle materials.

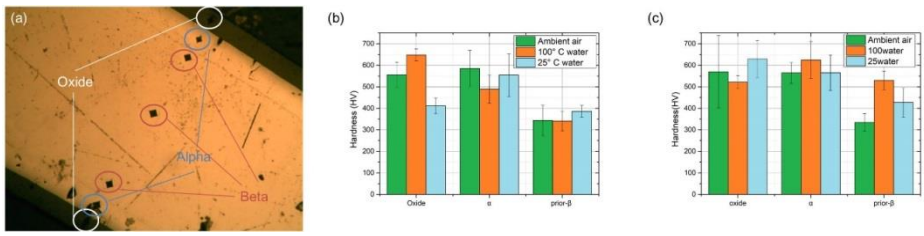

Figure 3-20. Vicker's hardness measurements of each phase layer (4 locations were measured). (a) indented location of hardness measurements, (b) as-received, (c) pre-hydrided specimens (765wppm),

RCT was conducted on tested specimens to examine residual cladding ductility. The obtained load-displacement results are shown in Fig. 3-21 (a) – (c), for each cooling condition, respectively.

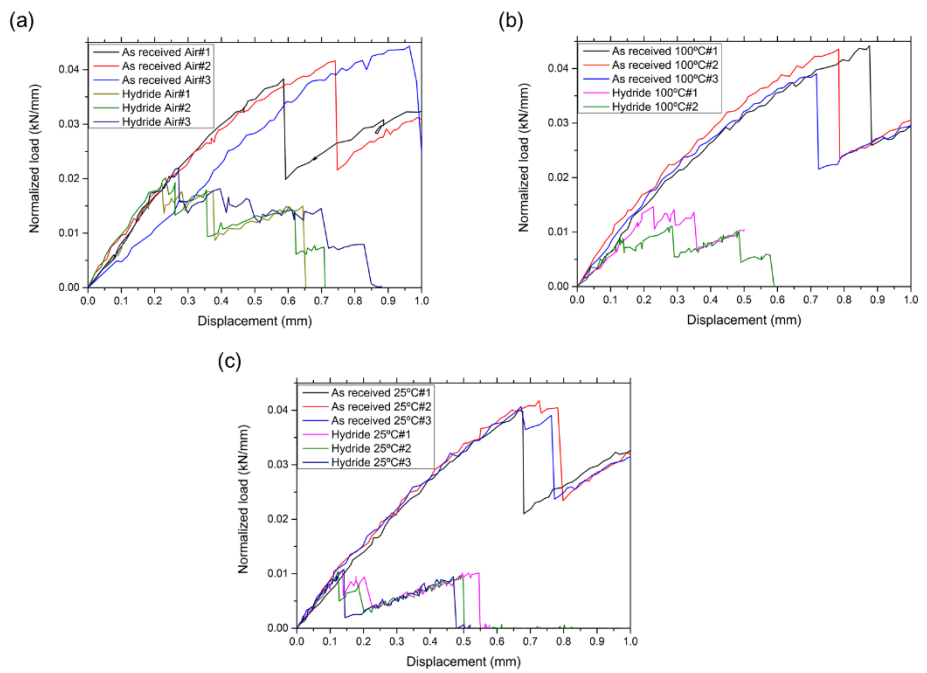

Fig. 3-21. Load-displacement curves of Ring Compression Test results. (a) air cooled, (b) 100°C water quenching, (c) 25°C water quenching

Table 3-3 summarizes offset strains and elastic moduli obtained from the load-displacement curves of Fig. 3-21 (a)-(c).

Table 3-3. Summary of RCT results

Sample No.	Hydrogen charged (wppm)	Quenching condition	Measured ECR(%)*	Average Offset strain (%)	Average Pseudo-Stiffness (kN/mm)	Average Fracture Load (kN)
1-1	As-received (~15wppm)	Ambient air	16.6%	1.58±0.51	0.63±0.13	0.32
1-2	As-received (~15wppm)	100ºC water	16.6%	2.79±0.34	0.64±0.04	0.33
1-3	As-received (~15wppm)	25ºC water	16.6%	1.45±0.16	0.58±0.02	0.31
2-1	765±19	Ambient air	16.4%	Nil ductility	0.69±0.13	0.15
2-2	765±19	100ºC water	16.4%	Nil ductility	0.46±0.05	0.089
2-3	765±19	25ºC water	16.4%	Nil ductility	0.65±0.01	0.073

* steam oxidation was conducted at 1204ºC for 275 seconds for all tested specimens.

Offset strain was evaluated at the first load drop. The DIC measurements shown in Fig.3-18 confirmed that the first load drop in the load-displacement curve corresponds to the first crack formation which takes place at either 12' or 6' location. Considering the inherent uncertainties of offset strain quantification (~1.5%), the average obtained offset strains (Table 3-3) exhibit limited sensitivity to cooling rates for as-received Zircaloy-4, with the difference of ~1%. Pre-hydrided specimens exhibited practically nil-ductility.

The cooling rate insensitivity on residual ductility can be explained by similar prior-β phase thicknesses (Fig. 3-16) and their oxygen contents (Fig. 3-17) irrespective of cooling rates. This implies that prior-β phase thickness and oxygen content dictate residual ductility. The observed incursion of α in prior-β phase and different microstructural lamellar thicknesses of prior-β phase (Fig. 3-18) do not introduce significant changes to average residual ductility. In addition, the presence of internal cracks, if any, in the oxide scales inferred from Fig. 3-20 (a) has negligible effect on

the residual ductility.

The high resolution DIC investigation with Gom-Correlate Professional 2019 analysis software demonstrates comparable local strain fields right before the first crack of RCT ($F=F_{fracture}$-5N, with applied force step of 5N) for 25°C water quench and 100°C water quench cases (Fig. 3-22). Ambient air cooled specimen shows a lower level of local strain fields right before cracking. Despite the apparent difference in the local strain fields, the global cladding mechanical behavior represented by the load-displacement curves (Fig. 3-21 (a) – (c)) demonstrate that the cooling rate has limited effect on the current regulatory framework which is based on the offset strain criteria.

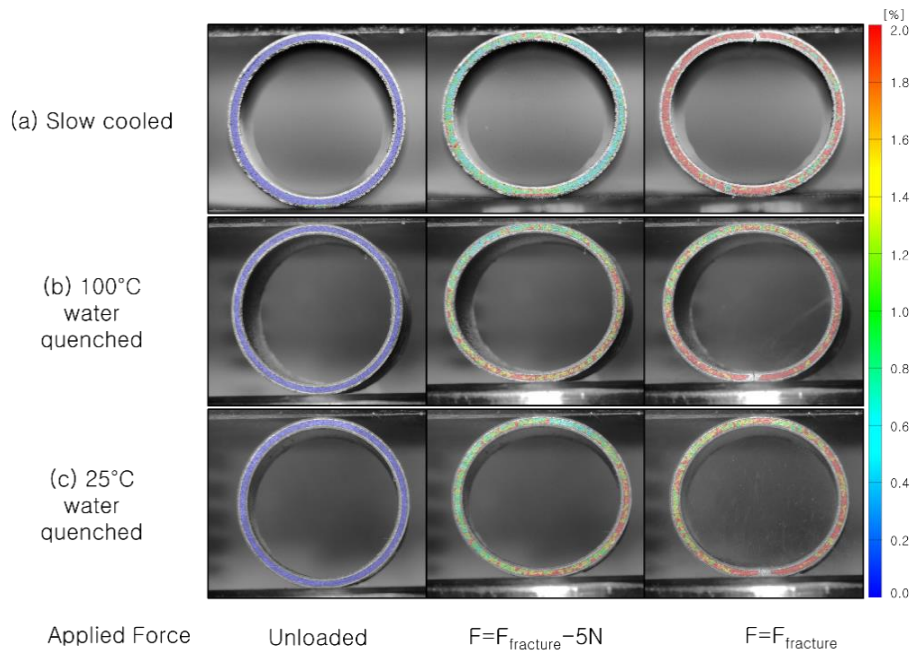

Figure 3-22. DIC results of von-Mises Strain for as-received Zircaloy-4 specimens (~17% ECR at 1204°C) undergoing RCT at 135°C

It is noteworthy that in Fig. 3-19 (a) – (c) variations of mechanical behavior among the tested specimens of the same cooling rate are markedly different. For all tested samples, air-cooling demonstrates substantially large deviations in load-displacement behavior among the tested specimens (Fig. 3-19 (a)) whereas both

water quenching cases exhibit a good agreement among the tested specimens (Fig. 3-19 (b) and (c)). Average load-displacement curves of the three tested specimens in each test are plotted in Fig. 3-16 to illustrate the statistical variations of the RCT results.

A notable feature inferable from fig 3-21 and table 3-3 is that the pre-hydrided specimens exhibit significantly larger difference in fracture strength. Such large difference of fracture strength found in the pre-hydrided materials are rooted in the statistical nature of brittle materials' strength. Dictated by pre-existing flaws without dislocation-mediated plasticity, brittle fracture occurs in a clearly statistical manner based on the population of pre-existing flaws and their distribution. Hence, pre-existing flaws in quantifying the mechanical strength are naturally higher for pre-hydrided cladding tubes. Nevertheless, it is important to note that the presented pre-hydrided cladding (765 wppm, ECR 17%) is unarguably brittle, making the uncertainties inconsiderable in terms of judging the residual ductility, compared to the specimen which has lower ECR and hydrogen concentration.

For as-received Zircaloy-4, faster cooling rate (i.e., 25°C water quench) clearly reduces variation among the tested specimens in the load displacement curves in terms of offset strain, pseudo-stiffness. Reduced α incursion in the prior-β phase and finer lamella microstructure of prior-β associated with rapid quenching (25°C) help homogenize prior-β phase, thereby reducing RCT uncertainty. This feature illuminates benefit of cold water quenching in reducing uncertainties of post-LOCA mechanical behavior.

3.4. Ring Compression Test strain rate

Sensitivity of applied strain rate of RCT on post-LOCA ductility has not been investigated. In order to standardize a specific strain rate, it is important to demonstrate that the applied strain rate ensures static testing that gives strain rate insensitive mechanical response. Hence, in addition to the pre-quenching cooling rate effect, this study investigates strain rate effect of RCT on post-LOCA cladding ductility assessment. By exploring two key unknowns on post-LOCA cladding ductility assessment, this study addresses regulatory implications and limitations of the current ECCS criteria.

Strain rate is known to have an influence on the flow stress. In general, material exhibits increasingly stiffer behavior with higher strain rate. Usually, strain rate of 10^{-5}-10^{-1} s^{-1} is known to correspond to static tension or compression tests while 10^{-1}-10^{2} s^{-1} is for dynamic tension or compression tests. A number of RCTs for post-LOCA ductility assessment applied different strain rates. The prototypic crosshead speed of the U.S NRC's post-LOCA ductility assessment was 2 mm/min which gives strain rate of ~3.5 x 10^{-3} s^{-1} for the as-received cladding diameter of 9.5mm. Study conducted by CEA used the crosshead speed of 0.5mm/min, giving strain rate of 8.7 x 10^{-4}~3.5 x 10^{-3} s^{-1}.

In order to standardize the test protocol, it is important to confirm that the RCTs are conducted in a static mode, giving strain rate-insensitive mechanical response. To experimentally confirm it, experimental investigation on the mechanical behavior of post-LOCA specimens with respect to different strains for various levels of ECRs (As-received, 10%, 17%) was conducted, and Fig. 3-23 shows the result. Fracture stress and fracture strain indicates the stress and strain values at the point of fracture (major load drop) in stress-strain curve. As can be noted, applied strain rate range of 1.0 x 10^{-3} – 6.0 x 10^{-3} s^{-1} ensures strain rate insensitive mechanical response. This result confirms the sanity of the prototypic strain rate (3.5 x 10^{-3}) used for post-LOCA ductility assessment.

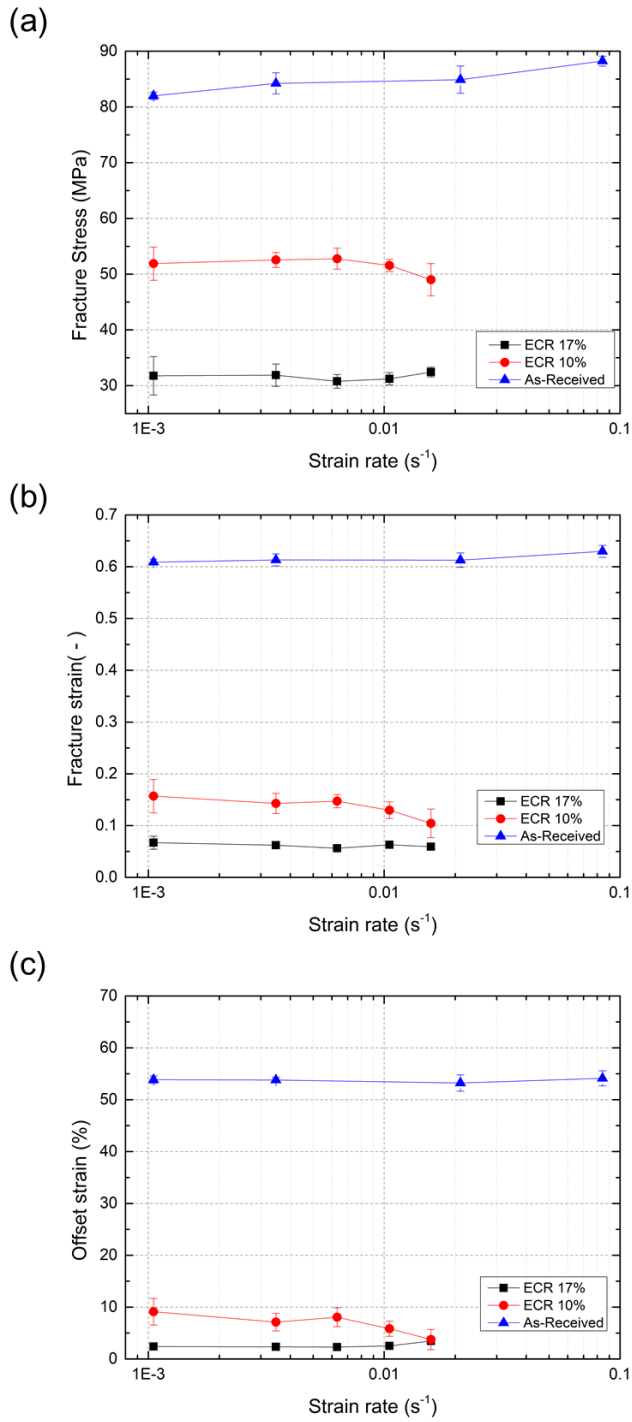

Figure 3-23. Measured Ring Compression Test parameters with various strain rate.

(a) Fracture stress, (b) Fracture strain, (c) Offset strain

Strian rate of Post-LOCA ductility test are suggested to be 0.0083mm/s ~ 0.033mm/s. usually 0.033mm/s is used to test cladding ductility. This strain rate is used in other general material strength test, but the suitability in the evaluation of residual ductility of cladding after coolant loss accident has never been evaluated.

It is well known that the plastic deformation of a metal material is affected by the high strain rate. And accordingly, it is necessary to quantitatively investigate the effect of the high strain rate on the ductility evaluation of the zirconium alloy cladding tube. By experimentally observing the sensitivity of the ductility evaluation result according to strain rate, the physical and regulatory suitability of the current RCT strain rate was identified.

LOCA experiment and RCT were performed on 8mm long ZIRLO as-received cladding. After the specimen was oxidized with steam at 1204℃ using a LOCA facility, specimen was cooled in air. Fracture stress, fracture strain, and offset strain of the cladding tube were measured at a strain rate of 0.01-1mm/s through the RCT, and the results are shown in Fig. 3-21.

3.5. Ring Compression Test temperature

135℃ is the lowest temperature that the cladding tube finally reaches after reflood in the event of LOCA. It is widely known that brittleness of metals increases with lower temperatures, and it is shown in Hobson's early experiments that this principle applies equally to zirconium cladding. In such background, the RCT temperature of 135°C is seen as a suitable criterion to ensure cladding ductility in all situations.

However, the assumption that the cladding will actually break due to a specific impact after LOCA, which has already reached 135°C, can seem to be overly conservative. In fact, the situation in which the cladding tube receives the greatest thermal shock is when quenching of the cladding tube occurs during reflood, and the literature suggests that the cladding will receive the greatest thermal shock at about 450℃, or at about 200℃, in this study.

The experimental results showed that the RCT at 200°C had higher ductility than the existing 135°C results in both hydrogen concentration of 209±17wppm, ECR 12.0% and hydrogen concentration of 486±12wppm, and ECR 5.9% (Fig. 3-24). Despite the fact that temperature difference is only 65°C, it can be seen that the oxidation limit guaranteed by the pre-hydrided cladding tube is greatly expanded, which can be suggested as an alternative to the oxidation limit applied to the current high burnup cladding.

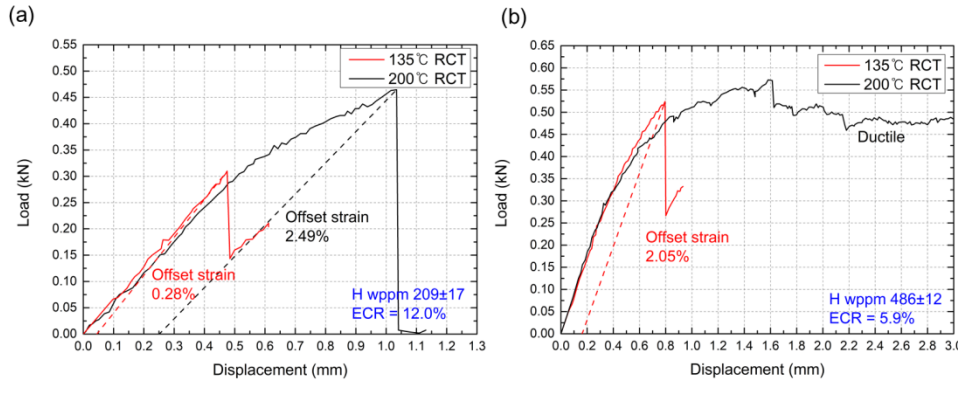

Figure 3-24. RCT results for different temperatures. (a) H concentration 209±17wppm, ECR 12.0% and H concentration 486±12wppm, and ECR 5.9%

3.6. Specimen length

* This study is done by S. Bang, and only the background results are cited in order to improve the completeness of this thesis.

Regarding the ductility evaluation after LOCA, regulatory guide suggests that length of the cladding before oxidation is at least 25 mm and the recommended length is 30 mm. This is to ensure that the number of specimens is stably 3 when the cladding is cut to 8 mm after oxidation. Therefore, it is recommended that the length of the cladding used in the loop compression test be 8 mm. The specimen used in the loop compression test is recommended to be 8 mm long, but in practice it is suggested to use the 7–10 mm.

Since the oxidized cladding is embrittled, fracture occurs probabilistically, rather than when a specific limit force or more is applied, as in the case of pre-oxidized cladding. Materials of this type can be explained by Weibull's formula. It describes the fracutre stress distribution of materials based on weakest link theory, which is sensitive to material volume.

Therefore, the specimen length is a very important factor in relation to the volume of the specimen in the RCT of oxidized cladding. And it is necessary to analyze how much the specimen length affects the overall results and what exactly the specimen length should be used in the experiment.

Using Weibull analysis, it was confirmed that the average offset strain tends to increase as the volume of the specimen decreases. Since the average offset strain of 8mm and 10mm specimens did not show any significant difference between the predicted and experimental values beyond the error range of the measured values, it was reasonable to recommend 7-10mm in the ductility test specimen. However, in the case of the 4mm specimen, it was confirmed that the average offset strain was about 60% greater than that of the 8mm specimen and the 10mm specimen. In other words, as predicted through weakest link theory, the offset strain increases as the

length of the specimen decreases, so there is a possibility that the residual ductility may be overestimated. Therefore, in order to exclude the effect of specimen size on the offset strain, it is more reasonable to limit the length of the specimen to a range (7-10 mm) but to fix it to a specific value (8 mm) during ductility evaluation.

3.7. Conclusion

• Effect of pre-quenching cooling rate

Effects of cooling rates and quenching temperatures on residual ductility of cladding after LOCA were investigated. In LOCA situation, Cladding has different cooling history by their axial location and accident scenario. This difference effects grain growth and hydride size of the cladding, resulting the difference on residual ductility. U.S.NRC regulatory guide suggests two options: ① Cool down to 800℃ with cooling rate over 2℃/s and quench, ② Direct quench. Since fast cooling rate has shown to lowering the cladding ductility, and it is hard to control all the regulatory experiments in same manner, it seems that regulatory body should have lenient attitude towards regulation

• Effect of cooling water temperature

Effects of cooling water temperature and according cooling rates on mechanical behavior of steam-oxidized Zircaloy-4 have been systematically investigated. Zircaloy-4 cladding specimens oxidized to the current U.S NRC's limits (17%ECR at 1204ºC) have been tested in order to draw regulatory implications. Quenching water temperature have (1) limited effects on average cladding residual ductility, and (2) pronounced effects on statistical variation of RCT results. The limited cooling-rate effect on residual ductility is due to the cooling-rate insensitive resulting phase thicknesses and their oxygen contents, both of which dictate the level of cladding residual ductility. Cooling rates affect both lamellar width and colony size, and α incursion in prior-β phase. These microstructural characteristics affect statistical variation of RCT results. Homogenizing prior-β phase with finer lamellar structures and reduced α incursion in prior-β phase, fast cooling (i.e., 25ºC water quenching) effectively reduces statistical variation of RCT results. this study confirms that results of past post-LOCA cladding ductility assessments conducted irrespective of quenching water temeprature can be used to support regulatory guidelines.

• Effect of RCT strain rate

The prototypic range of strain rate ($1.0 \times 10^{-3} – 6.0 \times 10^{-3}$ s^{-1}) for RCT is confirmed to yield 'static' tests that exhibit strain-insensitivity.

• Effect of RCT temperature

RCT temperature of 200°C showed enhanced ductility results in pre-hydrided cladding, which opened up the possibility for the less strict ECR limit for the high-burnup cladding.

• Effect of specimen length

Fixing the specimen length to 8mm was recommended, to get rid of the length effect on the Weibull distribution and fracture probability.

Suggested LOCA experiment and RCT protocols in this study are shown in table 3-7

Table 3-4. Suggested LOCA experiment and RCT protocols in this study

Suggested LOCA experiment protocols in this study		
	Value	**Physical validity**
Heating/cooling rate	Address 0.5℃/s ~ direct quenching	Ductility changes with cooling rate, LOCA situation have variety of cooling rates
Quenching temperature	1200℃ and 800℃	To simulate realistic reflood situation during LOCA
Quenching water	Either room temperature or boiling water	Thermal shock difference exists, but limited influence on residual ductility
Suggested Ring compression test protocols in this study		
Strain rate	0.033mm/s	Enough slow strain rate
RCT temperature	135℃	Temperature after the termination of LOCA
Specimen length	8mm	Length should be fixed

Chapter 4. Embrittlement limit of pre-hydrided ZIRLO and HANA claddings.

4.1. Deriving embrittlement limit of pre-hydrided ZIRLO and HANA claddings.

LOCA-simulating experiment following U.S.NRC protocols using pre-hydrided ZIRLO and HANA specimen was done, to find ductile limit of both Zircaloy cladding compositions. 30mm cladding was oxidized to several different ECR near ductile ECR limit, and cooled with cooling rate of 2℃/s and quenched at 800℃. After oxidation, cladding was cut into three 8mm specimen and conducted RCT at 135℃. All the results are shown in table 4-1.

Table 4-1. Ductile test results of different Hydrogen content and different ECR. Each line indicates the average of three 8mm specimens.

Cladding type	Hydrogen Content(wppm)	WG-ECR(%)	CP-ECR(%)	Av. Offset strain(%)	Ductility Assessment
ZIRLO	-	18.91	19.02	2.93	Ductile
	-	17.82	18.01	3.14	Ductile
	-	17.05	17.03	5.72	Ductile
ZIRLO	88.2	13.84	13.61	0.92	Brittle
	88.2	11.56	11.73	0.45	Brittle
	108.9	10.47	10.17	7.5	Ductile
	108.9	7.84	8.33	11.11	Ductile
ZIRLO	191.2	11.08	11.04	0.48	Brittle
	191.2	10.03	10.05	1.31	Brittle
	185.9	8.82	9.08	2.21	Ductile
ZIRLO	389.1	7.21	7.36	3.19	Transitional
	389.1	6.76	6.63	8.9	Ductile
	422.3	6.36	5.9	9.24	Ductile
	422.3	5.49	5.28	13.83	Ductile
ZIRLO	581.3	6.07	6.01	0.84	Brittle
	581.3	5.11	4.83	1.62	Brittle
	630.1	3.84	3.76	2.41	Ductile
HANA	-	19.13	19.02	2.84	Ductile

	-	17.63	18.01	3.04	Ductile
	-	16.97	17.03	6.49	Ductile
HANA	48.7	14.6	14.9	1.1	Brittle
	48.7	13.7	13.9	3.24	Ductile
HANA	148.8	11.8	13.18	0.48	Brittle
	148.8	10.99	11.96	0.83	Brittle
	158.1	10.23	10.82	0.82	Brittle
	158.1	9.03	9.61	2.58	Ductile
HANA	230.6	10.96	11.23	0.31	Brittle
	230.6	9.43	9.61	0.45	Brittle
	257.3	8.16	7.80	1.34	Brittle
	257.3	6.95	6.83	2.51	Ductile
HANA	618.8	7.71	7.10	0.57	Brittle
	618.8	5.71	5.84	1.67	Brittle
	572.7	5.09	4.62	2.04	Ductile

Ductile limit was constructed following the expreimental protocols of U.S.NRC. Ductile limit was found between ductile-brittle or transitional-ductile specimen. For example, specimen with Hydrogen content between 80wppm-120wppm was regareded as 100wppm spcimen. By using brittle specimen of ECR 11.73%, average offset strain 0.45%, and ductile specimen of ECR 10.17% and average offset strain 7.5%, we can derive ductile limit between two points, by using offset strain limit suggested in NRC regulatory guide, as shown in fig. 4-1.

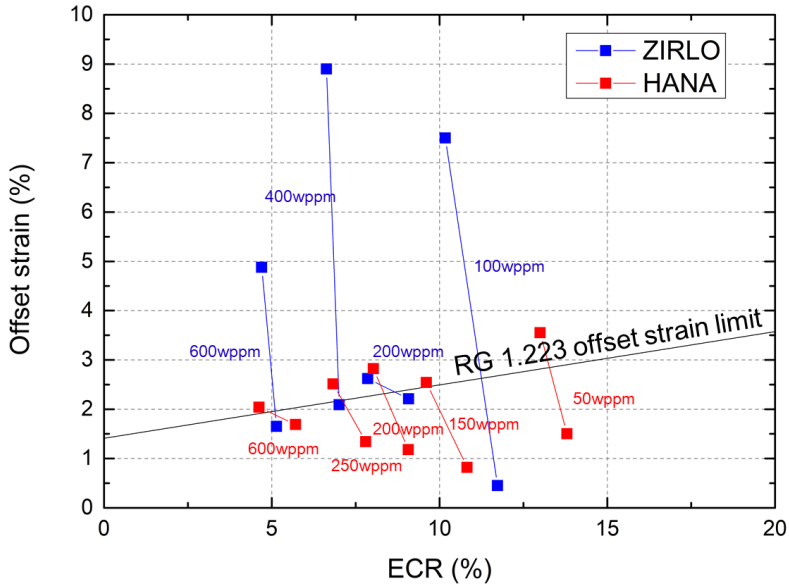

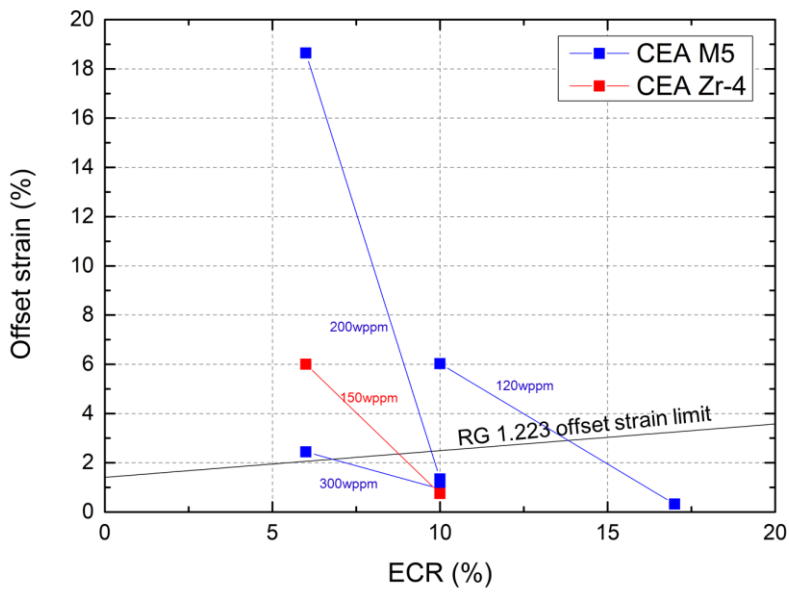

Figure 4-1. Derived ductile ECR limit from RCT offset strain results of (a) SNU, (b) CEA

Ductile limit points derived from RCT results are projected in fig. 4-2. As-received cladding shows slightly enhanced ductile limit than NRC draft rule, but pre-hydrided

cladding ranging from 50wppm to 250wppm shows clearly decreased ECR limit. But again, Hydrogen content ranging from 400 to 600 shows good agreement with NRC draft rule.

CEA has done post-LOCA ductility experiment of using pre-hydrided specimens. By deriving the ductile ECR limits by CEA data, they showed similar results with SNU. To explain the difference SNU/CEA and NRC data, experimental conditions of each facility has been done, and shown in table 4-2.

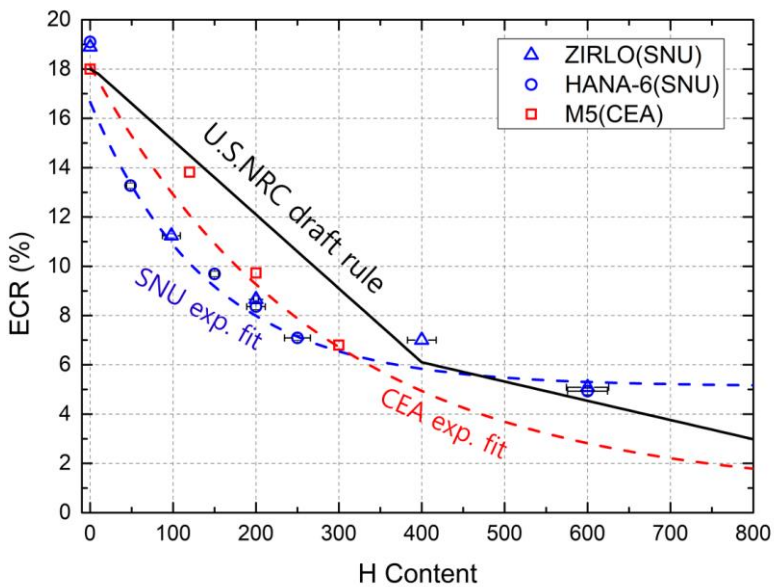

Figure 4-2. Ductile limit derived from pre-hydrided ZIRLO, HANA cladding

Primary difference in three facilities were ramping and cooling rate. Since cooling rate plays an important role in residual ductility of pre-hydrided cladding, slow cooling rate of CEA can act as a function of increasing ductility. However, CEA data has shown little difference with SNU data even though they had slower cooling rate.

Other difference in experimental conditions, such as ECR calculation, temperature measurement, specimen length, ductility assessment criteria, seemed to be minor

aspects in post-LOCA ductility compared with cooling rate.

This result of CEA implies that residual ductility of the cladding is not only affected by the experimental conditions, but also other unexpected aspects can affect the results.

Table 4-2. Comparison between different experiment facilities, ANL/CEA/SNU

		ANL(NRC)	CEA	SNU
Cladding material		ZIRLO/M5/ Zr-4	ZIRLO/M5	ZIRLO/HANA
LOCA experiment	**Ramping/ cooling rate**	>20℃/s to 1200℃ / **12℃/s to 800**	40℃/s to 1200℃ / **0.4℃/s to 800℃**	30℃/s to 1200℃ / **3℃/s to 800℃**
	ECR calculation	**CP-ECR integration**	**Weight gain**	**CP-ECR integration**
	Temperature measurement	**Attatched Thermocouple**	**Pyrometer**	**Attatched Thermocouple**
RCT	**Crosshead speed**	2mm/min	0.5mm/min	2mm/min
	Temperature	135℃	135℃	135℃
	Specimen length	7-10mm	10mm	7-9mm
	Specimen number	3EA per ECR	1EA per ECR	3EA per ECR
	Ductility assessment	Ductile/Brittle /Transitional	2% offset strain	Ductile/Brittle /Transitional

4.2. RCT in different temperature

This gap between NRC draft rule and derived limit of ZIRLO, HANA is not ignorable, since this difference of ~ECR 3% at 200wppm indicates ~75seconds of oxidation time. But this gap can also be explained by the RCT environment temperature. Current RCT temperature of 135℃ was selected by the fact that the water temperature after the termination of LBLOCA is 135℃, in accordance with core pressure of 3.2bar. But when core pressure is increased to 4.8bar, this RCT temperature can be changed to 150℃. In this study, RCT temperature of 150℃, 170℃, 190℃ was tried to find oth the temperature that can satisfy NRC draft rule. Results are shown in table 4-3.

Table 4-3. Ductile test results of different Hydrogen content with embrittlement limit ECR. Each line indicates the average of three 8mm specimens.

Cladding type	Hydrogen Content(wppm)	WG-ECR(%)	CP-ECR(%)	RCT Temp(℃)	Av. Offset strain(%)	Ductility Assessment
HANA	106.1	14.39	15.01	150	2.04	Brittle
				170	4.24	Ductile
				190	11.72	Ductile
HANA	188.5	11.39	12.03	150	1.43	Brittle
				170	3.17	Ductile
				190	8.31	Ductile
ZIRLO	251.8	10.00	10.55	150	0.28	Brittle
				170	1.23	Brittle
				190	15.19	Ductile
HANA	294.7	8.81	9.33	150	0.55	Brittle
				170	1.07	Brittle
				190	2.83	Ductile

For each hydrogen content of 100wppm, 200wppm, 250wppm, 300wppm, temperature satisfying NRC draft rule was drawn by comparing offset strain limit and offset strain results by RCT(fig 4-3) at each temperature, as shown in Fig. 4-4. Derived temperatures were 159℃ for 100wppm, 164℃ for 200wppm, 171℃ for 250wppm, 185℃ for 300wppm. Since 150℃ indicates steam pressure of 4.8bar and 190℃ indicates 12.5bar, the difference between 135℃ and 190℃ can be justified

by the little core pressure difference. This results are shown in Fig 4-5.

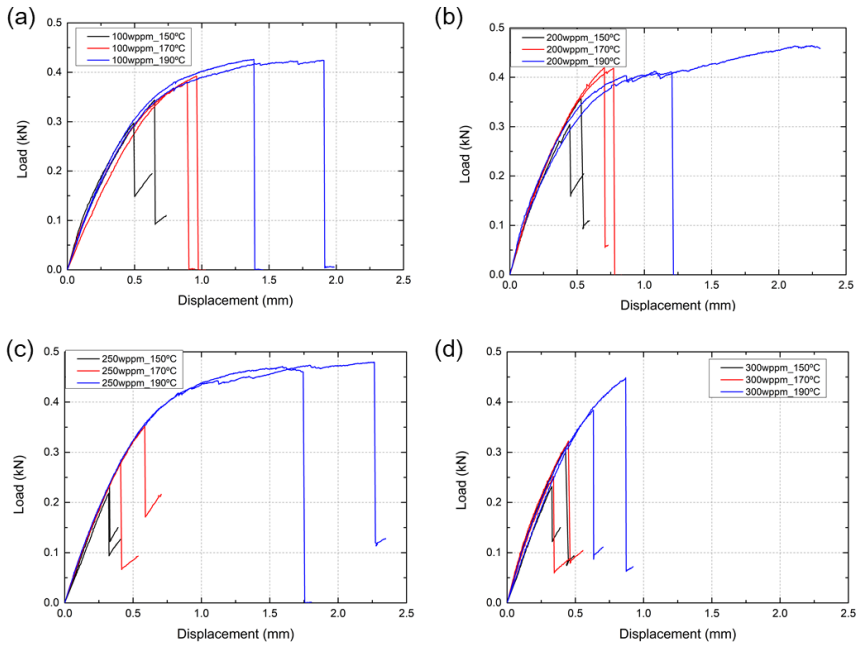

Figure 4-3. 150℃, 170℃, 190℃ temperature RCT results for (a) 100wppm, (b) 200wppm, (c) 250wppm, (d) 300wppm

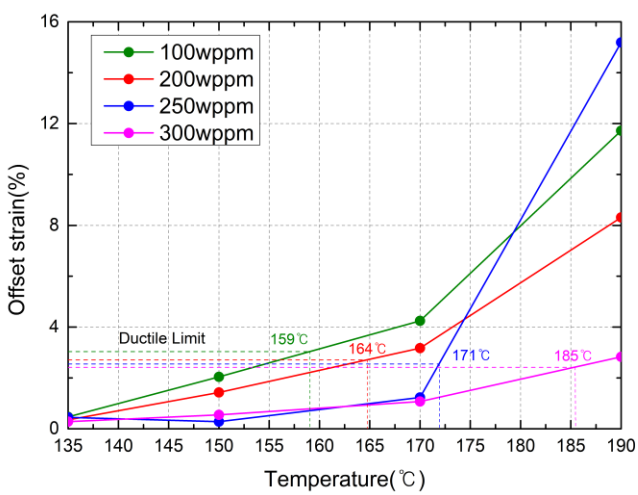

Figure 4-4. Deriving ductile temperature limit for cladding at ductile-brittle boundary

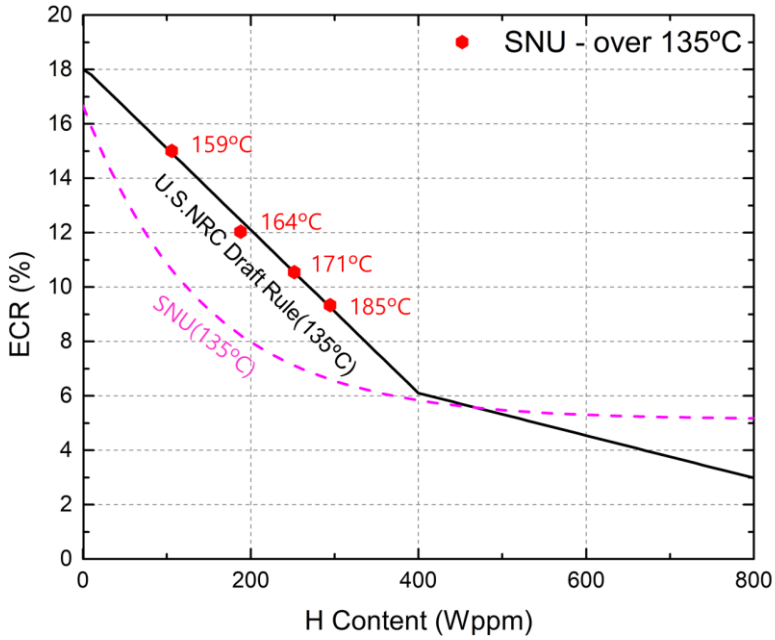

Figure 4-5. Comparing SNU-ECR limit with RCT results of different temperatures.

4.3. Conclusion

ECR limits of pre-hydrided ZIRLO, HANA cladding has been derived. Two different composition of cladding had similar ductility limit, but this limit had a gap between NRC draft rule between Hydrogen content 50wppm~250wppm. Definite cause for this gap has not yet been clearly investigated, since CEA test results showed same with SNU results. Nevertheless, it has two implications.

As-received specimen shows same ECR limit with NRC draft rule. For Cr-coated cladding, which has little degradation during plant operation, this result can be used as meaningful data when licensing purpose.

Pre-hydrided and oxidized specimen which has been brittle at 135℃ was turned to ductile when it became 160℃-185℃. Ductility of the cladding is significantly affected by RCT environment temperature, and only 25℃-50℃ difference has shown to be enough temperature for cladding to be turned to ductile from brittle. Again, regulatory body should have lenient attitude not only for cooling conditions, but also other experimental conditions such as RCT temperature.

Chapter 5. Summary of Conclusions

5.1. Summary of conclusions

• Comparative study between Thermal shock fracture-based and Ductility-based criteria, for high-burnup cladding has been conducted

Discrepancy between ductility-based and fracture-based ECCS criteria was explained. During LOCA trainsient, reflood quenching and thermal shock occurs rapidly so that slow hydrogen precipitation does not occur until the end of quenching. Therefore, fracture-based ECCS criteria maintained same ECR level for high-burnup claddings. Ductility-based criteria is based on ring compression test in 135℃ and cladding is embrittled due to the precipitation of hydrogen. Ductility-based ECCS criteria could not maintain its embrittlement ECR level for high-burnup claddings.
It is worth noting that these differences in regulatory perspective have caused a big difference in the cladding integrity assessment.

• Experimental protocols for ductility-based criteria has been revised

①Pre-quenching cooling rate

Effects of cooling rates and quenching temperatures on residual ductility of cladding after LOCA were investigated. In LOCA situation, Cladding has different cooling history by their axial location and accident scenario. This difference effects grain growth and hydride size of the cladding, resulting the difference on residual ductility. Since fast cooling rate has shown to lowering the cladding ductility, and it is hard to control all the regulatory experiments in same manner, it seems that regulatory body should have lenient attitude towards regulation

②**Cooling water temperature**

Effects of cooling water temperature and according cooling rates on mechanical behavior of steam-oxidized Zircaloy-4 have been systematically investigated. Quenching water temperature have (1) limited effects on average cladding residual ductility, and (2) pronounced effects on statistical variation of RCT results. Cooling rates affect both lamellar width and colony size, and α incursion in prior-β phase. These microstructural characteristics affect statistical variation of RCT results. This study confirms that results of past post-LOCA cladding ductility assessments conducted irrespective of quenching water temeprature can be used to support regulatory guidelines.

③**Effect of RCT strain rate**

The prototypic range of strain rate ($1.0 \times 10^{-3} – 6.0 \times 10^{-3}$ s^{-1}) for RCT is confirmed to yield 'static' tests that exhibit strain-insensitivity.

④ **Effect of RCT temperature**

RCT temperature of 200°C showed enhanced ductility results in pre-hydrided cladding, which opened up the possibility for the less strict ECR limit for the high-burnup cladding.

⑤**Effect of specimen length**

Fixing the specimen length to 8mm was recommended, to get rid of the length effect on the Weibull distribution and fracture probability.

• Ductile ECR limits of pre-hydrided HANA and ZIRLO cladding has been derived

ECR limits of pre-hydrided ZIRLO, HANA cladding has been derived. Two different composition of cladding had similar ductility limit, but this limit had a gap between NRC draft rule between Hydrogen content 50wppm~250wppm. Definite cause for this gap has not yet been clearly investigated, since CEA test results showed same with SNU results. As-received specimen shows same ECR limit with NRC draft rule. For Cr-coated cladding, which has little degradation during plant operation, this result can be used as meaningful data when licensing purpose. Pre-hydrided and oxidized specimen which has been brittle at 135℃ was turned to ductile when it became 160℃-185℃. Ductility of the cladding is significantly affected by RCT environment temperature, and only 25℃-50℃ difference has shown to be enough temperature for cladding to be turned to ductile from brittle. Again, regulatory body should have lenient attitude not only for cooling conditions, but also other experimental conditions such as RCT temperature.

Bibliography

[1] "Title 10, Energy, Parts 0 to 50" U.S.Code of Federal Regulations, Revised August 29, 2017. https://www.govinfo.gov/app/details/CFR-2017-title10-vol3/CFR-2017-title10-vol3-sec436-24/context

[2] P. Ihle, K. Rust, "SEFLEX. Fuel rod simulator effects in flooding experiments. Part 1. Evaluation Report." 1986. https://doi.org/10.5445/IR/270022572

[3] P. Ihle, K. Rust, "FEBA. Flooding experiments with blocked arrays. Evaluation Report" 1984. https://doi.org/10.5445/IR/270019863

[4] D.A. Powers, R.0. Meyer, "Cladding Swelling and Rupture models for LOCA Analysis" NUREG-0630, 1980. https://www.nrc.gov/docs/ML0534/ML053490337

[5] C. Greandjean, "Considerations and questions raised from a review of past and recent R&D work" NRC/IRSN Meeting 2007, 2007. https://www.nrc.gov/docs/ML0534/ML053490337.pdf

[6] A. Bianco, C. Vitanza, M. Seidl, A. Wensauer, W. Faber, R. Macián-Juan, "Experimental investigation on the causes for pellet fragmentation under LOCA conditions" Journal of Nuclear Materials, Volume 465, pp. 260-267, 2015. https://doi.org/10.1016/j.jnucmat.2015.05.035

[7] O. Coindreau, F. Fichot, J. Fleurot, "Nuclear fuel rod fragmentation under accidental conditions" Nuclear Engineering and Design, Volume 255, pp. 68-76, 2013. https://doi.org/10.1016/j.nucengdes.2012.09.021

[8] D.O. Hobson, P.L. Rittenhouse, "Embrittlement of Zircaloy Clad Fuel Rods by Steam during LOCA Transients" ORNL-4758, 1972. https://doi.org/10.2172/4670175

[9] D.O. Hobson, "Ductile-brittle behavior of Zircaloy fuel cladding. In: Proc. ANS Topical Mtg. on Water Reactor Safety, Salt Lake City, March 26, 1973, pp. 274–288, 1973. https://www.osti.gov/servlets/purl/4569664

[10] M. Billone, Y. Yan, T. Burtseva, R. Daum, "Cladding Embrittlement During Postulated Loss-of-Coolant Accidents" NUREG/CR-6967, 2008. https://doi.org/10.2172/946677

[11] G.R. Rajkumar, M. Krishna, H.N. Narasimhamurthy, Y.C. Keshavamurthy, J.R. Nataraj, "Investigation of Tensile and Bending Behavior of Aluminum based Hybrid Fiber Metal Laminates" Procedia Materials Science, Volume 5, pp. 60-68, 2014. https://doi.org/10.1016/j.mspro.2014.07.242

[12] B. Guo, Q. Zhao, M.J. Jackson, "Ultrasonic vibration-assisted grinding of micro-structured surfaces on silicon carbide ceramic materials" Proceedings of the Institution of Mechanical Engineers, Part B: Journal of Engineering

Manufacture, volume 226, issue 3, pp. 553-559, 2012. https://doi.org/10.1177/0954405411423574

[13] M. Billone, "Ductility Determination using Ring-Compression Tests" NRC Public Meeting, Draft Regulatory Guides DG-1261-1263, ORNL, 2015. https://www.nrc.gov/docs/ML1511/ML15111A204.pdf

[14] R.A. Holt, "The beta to alpha phase transformation in zircaloy-4" Journal of Nuclear Materials, Issue 3, 322-334, p. Volume 35, 1970. https://doi.org/10.1016/0022-3115(70) 90216-3

[15] O.T. Woo, K. Tangri, "Transformation characteristics of rapidly heated and quenched zircaloy-4-oxygen alloys" Journal of Nuclear Materials, Volume 79, Issue 1, pp. 83-94, 1979. https://doi.org/10.1016/0022-3115(79)90435-5

[16] A.R Massih, T. Andersson, P. Witt, M. Dahlbäck, M. Limbäck, "Effect of quenching rate on the β-to-α phase transformation structure in zirconium alloy," Journal of Nuclear Materials, Volume 322, Issues 2–3, pp. 138-151, 2003. https://doi.org/10.1016/S0022-3115(03)00323-4

[17] Y. Ben Ammar, A. Aoufi, M. Darrieulat, "Influence of the cooling rate on the texture and the microstructure of Zircaloy-4 studied by means of a Jominy end-quench test" Materials Science and Engineering, Volume 556, pp. 184-193, 2012. https://doi.org/10.1016/j.msea.2012.06.077

[18] J. Ni, Y. Zhao, L. Wang, Z. Zhang, J. Xie, "Microstructure of Zircaloy-4 alloy during β phase quenching and determination of critical quenching diameter of its rods" Nuclear Materials and Energy, Volume 17, pp. 158-163, 2018. https://doi.org/10.1016/j.nme.2018.10.014

[19] Y. Lee, T.J. McKrell, M. S. Kazimi., "Thermal Shock Fracture of Hot Silicon Carbide Immersed in Water" Journal of Nuclear Materials, Volume 467, Part1, pp. 172-180, 2015. https://doi.org/10.1016/j.jnucmat.2015.09.020

[20] Y. Lee, T.J. Mckrell, M. S. Kazimi, "Thermal Shock Fracture Of Silicon Carbide and its Application to LWR Fuel Cladding Performance during Reflood" Nuclear Engineering and Technology, volume 45, issue 6, pp. 811-820, 2013. https://doi.org/10.5516/NET.02.2013.528

[21] D.J. Prakash, Y. Lee, "Heat transfer foot print on ceramics after thermal shock with droplet impingement: Development of thermal shock tolerant material with hydrophobic surface" AIP advances, pp. Volume 8, issue 6, 2018. https://doi.org/10.1063/1.5041809

[22] Y. Lee, J. Lee, H. NO, "Impacts of Transient Heat Transfer Modelling on Prediction of Advanced Cladding Fracture during LWR LBLOCA" Nuclear Engineering and Design, Volume 298, pp. 25-32, 2016.

https://doi.org/10.1016/j.nucengdes.2015.12.015

[23] V. Vandenberghe, J.C. Brachet, M.Le Saux, D.Gilbon, J. P.Mardon, B. Hafidi, 2010, “Influence of the Cooling Scenario on the Post-Quench Mechanical Properties of PreHydrided Zircaloy-4 Fuel Claddings After High Temperature Steam Oxidation (LOCA Conditions),” Proceedings of the International Topical Meeting on Light Water Reactor Fuel Performance, Orlando, FL, Sept 26–29, pp. 270–277.

[24] F.J. Erbacher, H.J. Neitzel, K. Wiehr, 1990, "Cladding deformation and emergency core colling of a pressurized water reactor in a LOCA : summary description of the REBEKA program", Num 4781, 21 p, https://doi.org/10.5445/IR/270029557

[25] J. Stuckert, M. Grosse, M. Steinbrueck, M. Walter, A. Wensauer, 2020, "Results of the QUENCH-LOCA experimental program at KIT, Journal of Nuclear Materials", Volume 534, 152143, https://doi.org/10.1016/j.jnucmat.2020.152143.

[26] J.V. Cathcart, R.E. Pawel, R.A. McKee, R.E. Druscel, G.J. Yurek, J.J. Cambell, S.H. Jury, “Zirconium Metal-Water Oxidation Kinetics IV. Reaction Rate Studies” ORNL/NUREG-17, 1977.https://doi.org/10.2172/7317596

[27] S. Leistikow, S.G.Schanz, “The Oxidation Behavior of Zircaloy-4 in Steam between 600 and 1600 C” Materials and Corrosion, 36, pp. 105-116, 1985. https://doi.org/10.1002/maco.19850360302

[28] H. Chung, “Fuel behavior under loss-of-coolant accident situations” Nuclear Engineering and Technology, issue 37, 327-362, pp. 327-362, 2005.

[29] M. Négyesi, J. Burda, O. Bláhová, S. Linhart, V. Vrtílková,, “The influence of hydrogen on oxygen distribution inside Zry-4 fuel cladding” Journal of Nuclear Materials, Volume 416, Issue 3, pp. 288-292, 2011. https://doi.org/10.1016/j.jnucmat.2011.06.013

[30] J. Desquines, D. Drouan, S. Guilbert, P. Lacote, 2016, Embrittlement of pre-hydrided Zircaloy-4 by steam oxidation under simulated LOCA transients, Journal of Nuclear Materials, Volume 469, Pages 20-31, https://doi.org/10.1016/j.jnucmat.2015.11.008.

[31] Y. Udagawa, F. Nagase, T. Fuketa, “Effect of Cooling History on Cladding Ductility under LOCA Conditions” Journal of Nuclear Science and Technology, 43, 8, pp. 844-850, 2006. https://doi.org/10.1016/0022-3115(79)90172-7

[32] M.C. Billone, “Assessment of Current Test Methods for Post-LOCA Cladding Behavior” USNRC, NUREG/CR-7139, 2012.

[33] M.F. Ashby, R.H. Jones, "Engineering Materials 1-An introduction to their properties and applications", Second edition, Butterworth Heinemann, 1996.

[34] E.Torres, J.Desquines, S.Guilbert, P.Lacote, M.C.Baietto, M.Coret, M. Blat, A. Ambard, Oxygen segregation in pre-hydrided Zircaloy-4 cladding during a simulated LOCA transient, 2017, EPJ Nuclear Sci. Technol. 3 27,https://doi.org/10.1051/epjn/2017020

[35] K. Keum, Y. Lee, Effect of cooling rate on the residual ductility of Post-LOCA Zircaloy-4 cladding, Journal of Nuclear Materials 541 (2020) 152405.

[36] S. Bang, Y. Lee, The statistical ductility of embrittled Zircaloy-4 and its regulatory implications, Journal of Nuclear Materials, Volume 554, 2021, 153085, ISSN 0022-3115, https://doi.org/10.1016/j.jnucmat.2021.153085.

[37] Hyunwoo Yook, Youho Lee, Post-LOCA ductility assessment of Zr-Nb Alloy from 1100°C to 1300°C to explore variable peak cladding temperature and equivalent cladding reacted safety criteria,Journal of Nuclear Materials,Volume 567,2022,153829,ISSN 0022-3115, https://doi.org/10.1016/j.jnucmat.2022.153829.

[38] M. Billone, Y. Yan, T. Burtseva, R. Meyer, Cladding Behavior during Postulated Loss-of-Coolant Accidents, NUREG/CR-7219, March 2016

[39] USNRC. Regulatory Guide 1.223–Determining post quench ductility, Washington. D.C., USA, 2015.

[40] USNRC Regulatory Guide 1.224. Preliminary Draft (Draft was issued as DG-1263, dated March 2014), Establishing Analytical Limits for Zirconium-Alloy Cladding Material, Washington, (2018) 1–32.

[41] J. Brachet, V. Vandenbeghe, L. Portier, Hydrogen Content, Preoxidation, and Cooling Scenario Effects on Post-Quench Microstructure and Mechanical Properties of Zircaloy-4 and M5® Alloys in LOCA Conditions, Journal of ASTM International(2020), vol 5. No.4, 91-118, 10.1520/STP48132S

[42] V. Vandenberghe, J.C. Brachet, M. Le Saux*, D. Gilbon, M. Billonec, D. Hamon, J.P. Mardon, B. Hafidi, Influence of the Cooling Scenario on the Post-Quench Mechanical Properties of Pre-Hydrided Zircaloy-4 Fuel Claddings after high Temperature Steam Oxidation (LOCA Conditions),Proceedings of 2010 LWR Fuel Performance/TopFuel/WRFPM (2010), Paper 096

[43] J. Lee, S. Woo (2014), Effects of fuel rod uncertainty on the LBLOCA safety analysis with limiting fuel burnup change,Nuclear Engineering and Design, Volume 273, Pages 367-375, ISSN 0029-5493, https://doi.org/10.1016/j.nucengdes.2014.03.051.

[44] D. Kim, H. Yook, K. Keum, Y. Lee, TRANOX: Model for non-isothermal steam oxidation of Zircaloy cladding, J. Nucl. Mater. 556 (2021) 153-153.

[45] K. Wei, R. Hu, D. Yin, L. Xiao, S. Pang, Y. Cao, H. Zhou, Y. Zhao, Y. Zhu, Grain size effect on tensile properties and slip systems of pure magnesium, Acta Materialia, Volume 206, 2021, 116604, ISSN 1359-6454, https://doi.org/10.1016/j.actamat.2020.116604.

[46] A. Jain, O. Duygulu, D.W. Brown, C.N. Tomé, S.R. Agnew, Grain size effects on the tensile properties and deformation mechanisms of a magnesium alloy, AZ31B, sheet, Materials Science and Engineering: A, Volume 486, Issues 1–2, 2008, Pages 545-555, ISSN 0921-5093, https://doi.org/10.1016/j.msea.2007.09.069.

[47] S. Kim, J. Kang, Y. Lee, Hydride embrittlement resistance of Zircaloy-4 and Zr-Nb alloy cladding tubes and its implications on spent fuel management, Journal of Nuclear Materials, Volume 559, 2022, 153393, ISSN 0022-3115, https://doi.org/10.1016/j.jnucmat.2021.153393.

[48] W. Qin, N.K. Kumar, J.A. Szpunar, J. Kozinski, Intergranular δ-hydride nucleation and orientation in zirconium alloys, Acta Mater. 59 (18) (2011) 7010–7021, doi:10.1016/j.actamat.2011.07.0

[49] Chapman TP, Dye D, Rugg D.,2017 Hydrogen in Ti and Zr alloys: industrial perspective, failure modes and mechanistic understanding.Phil. Trans. R. Soc. A 375:20160418.,http://dx.doi.org/10.1098/rsta.2016.0418

[50] J. Lee,Y. Kim(2018),A Review of Factors Influencing the Hydride Reorientation Phenomena in Zirconium Alloy Cladding During Long-Term Dry Storage,Korean J. Met. Mater., Vol. 56, No.2 (2018), pp.1-14,DOI: 10.3365/KJMM.2018.56.2.1

[51] H. Conrad, S. Frederick(1962),The effect of temperature and strain rate on the flow stress of iron, Acta Metallurgica,Volume 10, Issue 11,Pages 1013-1020,ISSN 0001-6160,https://doi.org/10.1016/0001-6160(62)90070-6.

[52] Mechanical metallurgy, E. George, Bacon, David (2011), MCGraw-Hill,ISBN : 9780071004060

Abstract

고연소도 피복관의 비상노심냉각계통(ECCS) 허용기준에 대한 기술적 근거가 체계적으로 연구되었다.

두 가지 주요 실험인 열충격 파괴와 급냉 이후 연성 기반 실험을 비교하여 고연소도 피복관의 각 조건 하에서의 ECR 한계치 사이의 차이를 설명하였다. MARS 코드, GIFT 코드를 활용하여 피복관 온도, 응력, LOCA 상황 동안 석출된 수소의 양을 모두 계산하였다. LOCA 상황에서 재관수 급냉시 피복관의 응력은 약 200℃에서 최고점에 도달한다. 그 순간에, 수소의 석출량은 수소 석출 동역학에 의해 낮은 수준으로 유지된다. 연성 기반 실험에서는 135℃에서, 모든 수소가 석출된 상태로 고리압축시험(RCT)을 실시한다. 이러한 온도 차이(200℃와 135℃), 그리고 최대 하중 시 수소 석출량의 차이는 ECR 한계치의 차이를 초래하였다.

급냉 이후 연성 판단 기준 실험의 구체적인 실험 방법론의 절차를 살펴보았다. 급냉 전 냉각 속도, 급냉 온도, 냉각수 온도, 고리압축시험의 연신률, 고리압축시험시 온도, 시편 길이 등을 체계적으로 연구하였다. 급냉 전냉각 속도가 느릴수록, 합금 원소가 석출되고 큰 수소화물이 형성되어 피복관 연성이 증가하였다. 급냉 냉각수의 온도에 의해 급냉시의 냉각속도가 변했으며, 상온의 급냉수의 급속냉각으로 인해 속도로 열충격이 강화되었으나, 이는 피복재의 잔류연성에 제한적인 영향을 보였다. 고리압축속도 연신률 2mm/min은 연신률을 늦추거나 빠르게 하여도 피복관 연성이 영향을 받지 않는 충분한 느린 속도인 것으로 나타났다. 고리압축온도가 증가하면, 피복관의 연성이 증가하는 것으로 나타났다. 잔류 연성에 대한 시편 길이 효과를 없애기 위해 시료 길이를 8mm로 고정하는 것이 제안되었다.

HANA 및 ZIRLO 피복재의 취성 한도가 도출되었다. 수소 함량이 50~250wppm 피복관에서 ECR 한계가 미국보다 약간 낮게 나타났다. 수소 함량 400wppm ~ 650wppm 피복관은 미국 규제기관의 제한치와 유사한 결과를 보였다. RCT 온도 변화는 미국 규제기관의 제한치와 서울대 제한치 사이의 격차를 메우기 위해 제안되었다. 185℃의 RCT 온도는 두 제한치 사이의 간격을 채울 것으로 예상되었다.

이 연구의 결론으로, LOCA 이후 피복관의 잔류 연성을 평가하는 현재의 규제 실험 프로토콜이 재검토되었다. 규제 당국은 비상 노심 냉각 시스템에 대한 현실적인 규제 기준을 만들기 위해 실험 조건과 방법에 대해 관대한 시각을 가져야 할 것으로 보인다.

감 사 문

가장 먼저 지식과 경험이 많이 부족하던 저를 연구실의 일원으로 받아주시고, 본인의 지혜를 아낌없이 나누어주시고 열정을 다하여 지도해주신 이유호 교수님께 진심으로 감사의 인사를 드립니다. 발전해야 할 부분이 많고 손이 많이 가는 제자였지만, 필요한 순간 주셨던 격려의 말씀들과 핵심을 짚는 소중한 조언을 통해 미력하나마 연구자로서의 바른 길로 갈 수 있었습니다. 진심을 다해 이끌어주셔서 정말 감사드립니다. 기꺼이 심사를 맡아 주시고 졸업 연구의 완성도를 높이기 위한 조언을 아끼지 않으신 조형규 교수님과 박현선 교수님께도 감사의 인사를 드립니다.

대학에서 대학원으로 이어지는 긴 과정 동안 묵묵히 저의 뒷바라지를 해주시고, 힘든 일이 있을 때마다 상담해주신 부모님께 감사인사를 올리고 싶습니다. 부모님 덕분에 힘든 일들도 지나갈 수 있었고 졸업이라는 두 글자를 담을 수 있게 되었습니다.

새롭게 생긴 연구실을 함께 꾸려 나가며 여러 고생을 함께했던 상범이형, 동연이형, 현택이에게도 감사의 말씀을 전합니다. 또 오랜 시간 연구실에서 시간을 함께 보내며 동고동락했던 현우와 동주에게도 고맙다는 말을 하고 싶습니다. 도움이 필요했던 많은 순간에 아낌없이 도움을 주면서도 본인이 맡은 바를 늘 열심히 하던 연구실 후배들, 찬수, 동욱, 다현, 성훈, 승민, 종호, 규석, 창현, 윤성이에게도 감사의 인사와 대학원 생활에 대한 응원의 말씀을 전합니다. 또 늘 웃는 모습으로 조언과 격려를 해주신 이정현 박사님, 밝게 인사해주시며 힘을 주시던 김진수 박사님께도 감사의 말씀을 드립니다. 항상 묵묵히 연구실을 지원해주신 전효선선생님, 그리고 실험이 막힐 때마다 많은 실전적인 도움을 주신 지선이형께도 정말 감사 드립니다. 그리고 다 적진

못하지만, 대학원 생활 속에서 서로의 기쁨과 고충을 나누며 힘을 내게 해주었던 과 동기들, 산책을 함께했던 남재, 성빈, 주룡, 재성, 동규, 명건, 산, 인규, 진성, 현우에게도 고맙다는 말을 하고 싶습니다.

인턴을 시작했던 2019년 여름부터, 석사로 학교를 졸업하는 2022년 여름까지 짧다면 짧고, 길다면 길다고 할 수 있는 3년간 정말 많은 일들이 있었고 다양한 경험을 통해 한 사람으로서 제가 성장할 수 있었습니다. 이 모든 것은 제가 이룬 것이 아니라, 제가 헤매고 있어 힘들어할 때마다 도움을 주었던 수많은 분들이 이루어주신 것이라고 생각합니다. 다시 한번 감사의 말씀을 드리며 학교를 떠나서도 아껴주셨던 마음에 보답할 수 있도록 노력하는 삶을 살겠습니다.

2022년 7월
금경환 올림